Emerging thermal-responsive materials and integrated techniques targeting the energy-efficient smart window application

Ke, Yujie; Zhou, Chengzhi; Zhou, Yang; Wang, Shancheng; Chan, Siew Hwa; Long, Yi

2018

Ke, Y., Zhou, C., Zhou, Y., Wang, S., Chan, S. H., & Long, Y. (2018). Emerging Thermal-Responsive Materials and Integrated Techniques Targeting the Energy-Efficient Smart Window Application. Advanced Functional Materials, 28(22), 1800113-. doi:10.1002/adfm.201800113

https://hdl.handle.net/10356/105827

https://doi.org/10.1002/adfm.201800113

DOI: 10.1002/
Article type: Review

Emerging Thermal-Responsive Materials and Integrated Techniques Targeting the Energy-Efficient Smart Window Application

*Yujie Ke,[1] Chengzhi Zhou,,[2,3] Yang Zhou,[1] Shancheng Wang,[1] Siew Hwa Chan,[3] Yi Long.[1,4,] **

[1] School of Materials Science and Engineering, Nanyang Technological University, 50 Nanyang Avenue, 639798, Singapore
[2] Energy Research Institute @ NTU, Interdisciplinary Graduate School, Nanyang Technological University, 50 Nanyang Drive, 637553, Singapore
[3] School of Mechanical and Aerospace Engineering, Nanyang Technological University, 50 Nanyang Avenue, Singapore 639798, Singapore.
[4] Singapore-HUJ Alliance for Research and Enterprise (SHARE), Campus for Research Excellence and Technological Enterprise (CREATE), 1 Create Way, 138602, Singapore

Keywords: smart window, thermochromism, perovskite, metamaterial, hydrogel

Abstract

Architectural windows that smartly regulate indoor solar radiation by changing their optical transmittance in response to thermo-stimuli have been developed as a promising solution toward reducing the energy consumption of buildings. Recently, energy-efficient smart window technology has attracted increasing scientific interest, with the exploration of energy-efficient novel materials as well as integration with practical techniques to generate various desired multi-functionalities. This review systematically summarizes emerging thermo-responsive materials for smart window applications, including hydrogels, ionic liquids, perovskites, metamaterials, and liquid crystals. These are compared with vanadium dioxide (VO_2), a conventional and extensively studied material for thermochromic smart window applications. In addition, recent progress on cutting-edge integrated techniques for smart windows is covered, including electro-thermal techniques, self-cleaning, wettability and also

integration with solar cells for bifunctional energy conservation and generation. Finally, opportunities and challenges relating to thermochromic smart windows and prospects for future development are discussed.

1. Introduction

The growing world population and rapid modernization have led to increased energy demand, necessitating highly efficient energy use.[1] Building energy usage accounts for up to 40% of the overall energy consumption in developed countries, which exceeds the energy consumed by the industry and transportation sectors **(Figure 1a)**.[2] Building services including heating, ventilation and air conditioning (HVAC) are major components of building energy consumption, contributing approximately 50% of total building energy (Figure 1a).[2a] Reducing the energy consumption of these services whilst maintaining building comfort levels is a significant challenge in sustainable development.[3] Amongst all building components, windows are considered to be one of the least energy-efficient parts as there is always heat transfer in the opposite direction to that desired.[4]

In recent times, smart windows have received considerable attention because of their potentially significant contribution to the economization of building energy consumption.[5] A window can regulate indoor solar irradiation in a 'smart' way, that is, by dynamically and reversibly tuning the transmittance of ultraviolet (UV), visible, and infrared (IR) solar radiation.[6] Development of smart windows can mainly be categorized as electro-, thermo-, and photo-stimulated optical response changes **(Figure 1b)**.[7] Among them, smart windows based on thermoresponsive materials are highly competitive due to their unique characteristics: (1) low cost, arising from their simple configuration resulting in low fabrication and maintenance costs, especially compared to electrochromic smart windows which are composed of electrolyte, electrodes, require an additional power system and other

features (Figure 1b); (2) passivity, with their automatic response to temperature cutting down the need for switch systems, for example electrical control requiring external energy and human manipulation; (3) rational stimulus-response, with regulation by indoor temperature rather than UV-triggered optical modulation in photochromic materials.

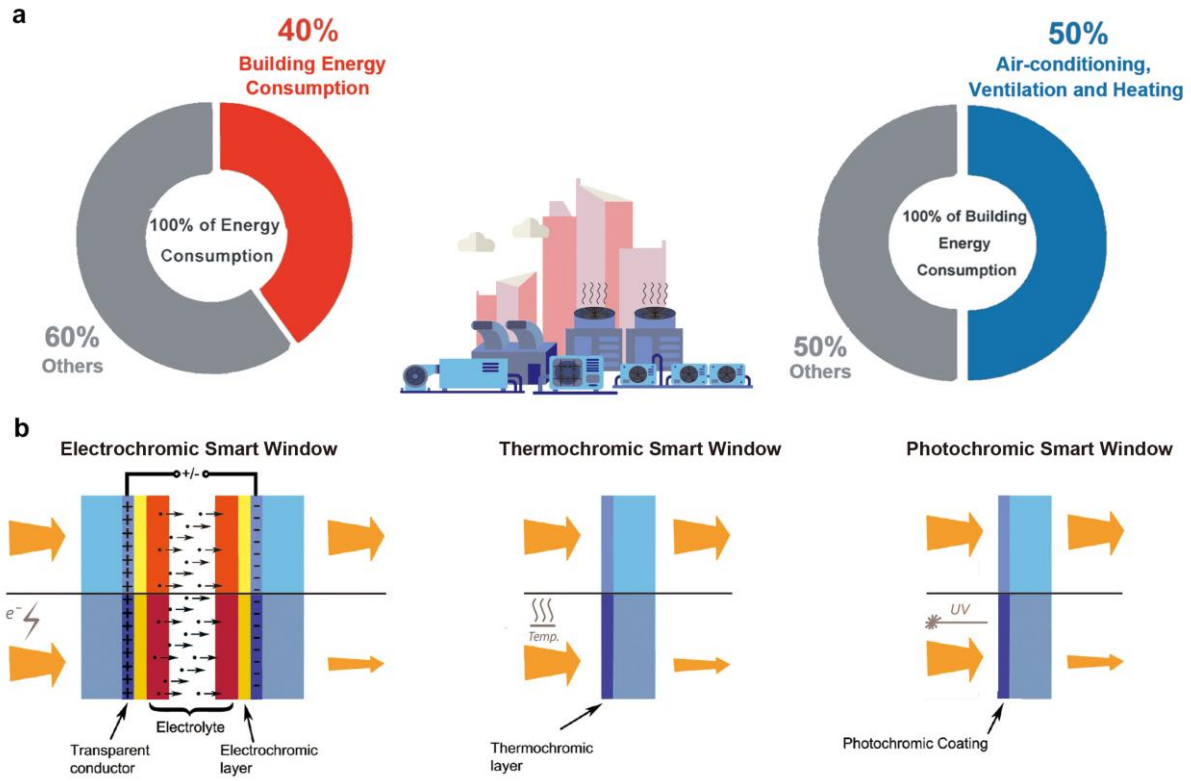

Figure 1. a) Proportion of building energy consumption compared with total energy consumption. Proportion of energy consumption of building services such as heating, ventilation, and air conditioning of total building energy consumption. b) Schematic of electrochromic, thermochromic and photochromic smart windows. The orange arrows indicate incident sunlight. Reproduced with permission.[7a] Copyright 2017, John Wiley & Sons.

Conventional studies of thermochromic smart windows have mainly focused on vanadium dioxide (VO_2), which undergoes a metal-insulator transition at the critical temperature (τ_c) of 68 °C, accompanied with huge transmittance contrast in the IR range and negligible change in the visible range.[8] The integrated luminous transmittance (T_{lum}) and the integrated solar energy modulation (ΔT_{sol}) are two key parameters to assess performance, for which calculation methods can be found in previous reports.[7a, 8] Extensive efforts have been put

into optimizing T_{lum} and ΔT_{sol} by nano/micro-scale engineering, including of porosity, nanocomposites, biomimetic design, grids and multilayers.[9] However, challenges regarding pure VO_2-based smart windows still remain regarding the relatively high τ_c intrinsic yellow-brown color and low resistance to oxidization; more importantly the unfavorable combination of low T_{lum} and ΔT_{sol}, which are less than 50% and 20% respectively in most researches.

There is emerging scientific interest in the exploration of new temperature-responsive materials. Feasible materials must be able to switch automatically between transmitted and scattered/blocked to solar radiation, with a huge contrast at cold and warm seasons. Other key considerations include a suitable transition temperature range (30-40 °C), outstanding durability, acceptable appearance, facile and low-cost of manufacture and maintenance. Additionally, various demands arising from the practical market have increased research attention on multifunctional smart windows as well as functional thermochromic devices, which could be achieved by integration with other state-of-the-art techniques.

In this review, emerging thermo-responsive materials for smart window applications are firstly outlined and discussed, including hydrogels, ionic liquids, perovskites, metamaterials, and liquid crystals **(Figure 2 right)**. The respective mechanisms of each material are presented with emphasis on the thermally induced optical property change. The following section is to further compare these materials with conventional thermochromic VO_2 (Figure 2 right). Subsequently, recent achievements in integrated techniques for thermoresponsive smart windows are summarized, including the electro-thermal technique, self-cleaning, wettability and integration with solar cells (SCs) for energy conservation and generation bifunctionality **(Figure 2 left)**. Finally, prospects for future development are discussed, from both material and integrated device perspectives. Considering the enormous library of thermoresponsive materials and integrated techniques, great opportunities in this field remain. The objective of

this review is to broaden research interests and inspire further innovative approaches to accelerate the development of energy-efficient smart window technologies.

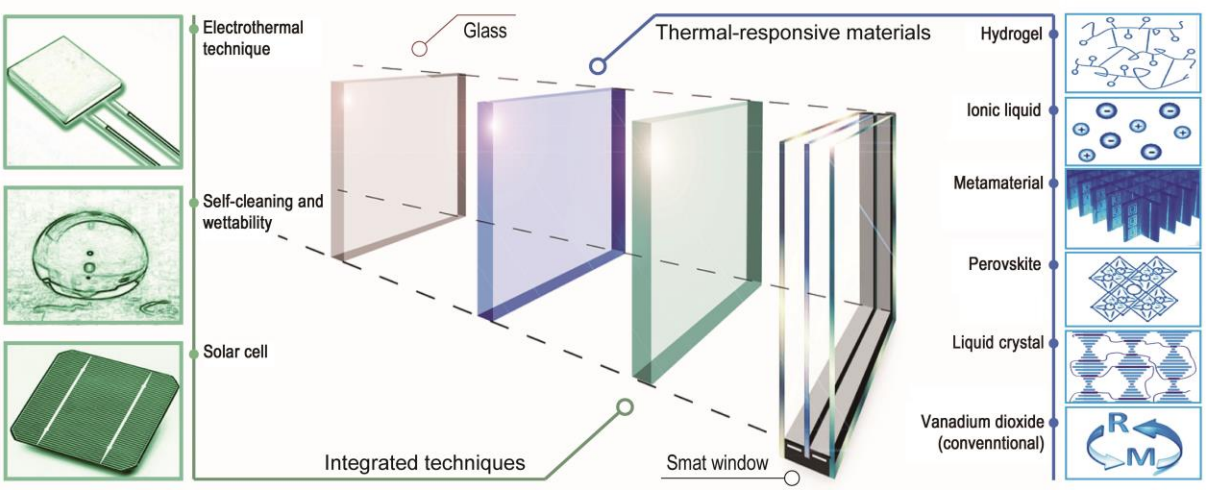

Figure 2. Schematic outline of the two key components of energy-efficient smart windows: thermoresponsive materials and integrated techniques. Emerging materials include hydrogels, ionic liquids, metamaterials, perovskites, and liquid crystals. The conventional VO_2 is briefly discussed as a reference.

2. Emerging thermal-responsive materials

2.1. Hydrogels

Hydrogels are networks of hydrophilic polymer chains with an aqueous rich environment which renders broadly tunable chemical and physical properties. The first hydrogel was demonstrated in 1894.[10] Nowadays, hydrogels have been applied in different areas, including tissue engineering,[11] drug delivery systems,[12] cell cultures,[13] and biological implants.[14] Recently, thermochromic hydrogels, a special category of hydrogels, have attracted considerable attention as a candidate for energy-efficient smart window applications. The extensively studied thermochromic hydrogels include polyampholyte hydrogel (PAH),[15] poly(N-isopropylacrylamide) (PNIPAm),[16] and hydroxypropyl cellulose (HPC).[17] Significantly, thermochromic hydrogels undergo a hydrophilic to hydrophobic transition **(Figure 3a)**: when the temperature is below the lower critical solution temperature (LCST), intermolecular hydrogen bonds are prevalent between the polymer chains and surrounding

water molecules; once the temperature increases above the LCST, intermolecular hydrogen bonds are broken, then polymer chains collapse, resulting in phase separation and polymer aggregation.[18] The aggregated polymer clusters reduce the transparency of the hydrogel by scattering incident light.[19] A polymer chain volume reduction of over 90% can be observed following the phase transition separation.[20]

This LCST characteristic makes thermochromic hydrogels promising candidates for energy-efficient smart windows. One of the most common configurations for hydrogel-based smart windows is the sandwich structure, where the thermochromic hydrogel is sandwiched between two pieces of glass substrate (**Figure 3b)**. Zhou *et al.* reported pure PNIPAm hydrogel based smart window, which has suitable LCST at ~32 °C;[16a] the LCST phase transition was found to affect a relatively large spectral range of light transmittance, as illustrated in **Figure 3c**. Specifically, a drastic transmittance contrast in response to temperature was observed from 250-1800 nm, while the temperature effect on transmittance after 1800 nm was relatively negligible. The difference in transmission was mainly due to the aggregation of polymer chains once temperature is above LCST.[18b, 21] The temperature-dependent optical properties of 200 μm PNIPAm hydrogel thin film is displayed in **Figure 3d**, including T_{lum}, ΔT_{sol}, calculated infrared modulation (ΔT_{IR}), and integrated visible light modulation (ΔT_{lum}). Below LSCT, the transparency of the PNIPAm hydrogel film was maintained well in both the visible light region and the NIR region. However, as the temperature increased above the LSCT, a significant drop of transmittance was observed throughout the entire spectrum. When the temperature was increased to 60 °C, T_{lum} fell to 60% and T_{IR} was reduced significantly to only 19.3%. Due to the rapid decrease of both T_{lum} and T_{IR}, a continuously decreasing T_{sol} was observed (from 83.3% to 9.4%). The result was that the 200 μm PNIPAm hydrogel thin film was observed to change from transparent at room

temperature to opaque above 35 °C (**Figure 3bi and 3bii**). The PNIPAm could be further embedded within a silica-alumina-based gel matrix for 3D printing process.[22] Another example is a PAH-based smart window,[15] which, instead of being transparent at low temperature was designed to be opaque at cold temperatures to retain indoor heat, which may be applicable particularly for winter nights.

Further explorations have been reported by Long *et al.* on hybrids of hydrogel with inorganic VO_2 particles.[16b] PNIPAm-VO_2 hybrid thin film was sandwiched between two pieces of glass substrate **(Figure 3e)**, with a demonstration of this film at room temperature and 35 °C shown in Figures 3ei and 3eii, respectively. The transmittance spectrum of pure hydrogel, pure VO_2 nanoparticles and the VO_2/hydrogel hybrid at 20 and 80 °C are shown in **Figure 3f**. Compared with pure hydrogel, ΔT_{sol} of the hybrid material was significantly improved, especially in the NIR region where a ΔT_{IR} of 22.2% was observed. The PNIPAm-VO_2 hybrid film also showed constant T_{lum} and ΔT_{sol}, as demonstrated by repeated heating and cooling process on a 100 μm film between 20 and 80 °C for 20 cycles **(Figure 3g)**. Furthermore, compared with pure VO_2 nanoparticles the hybridized system demonstrated higher luminous transmittance at both room temperature and elevated temperature. The same research group also applied less noxious HPC hydrogel to thermochromic foils that were responsive near room temperature by compositing with tungsten-doped VO_2.[17]

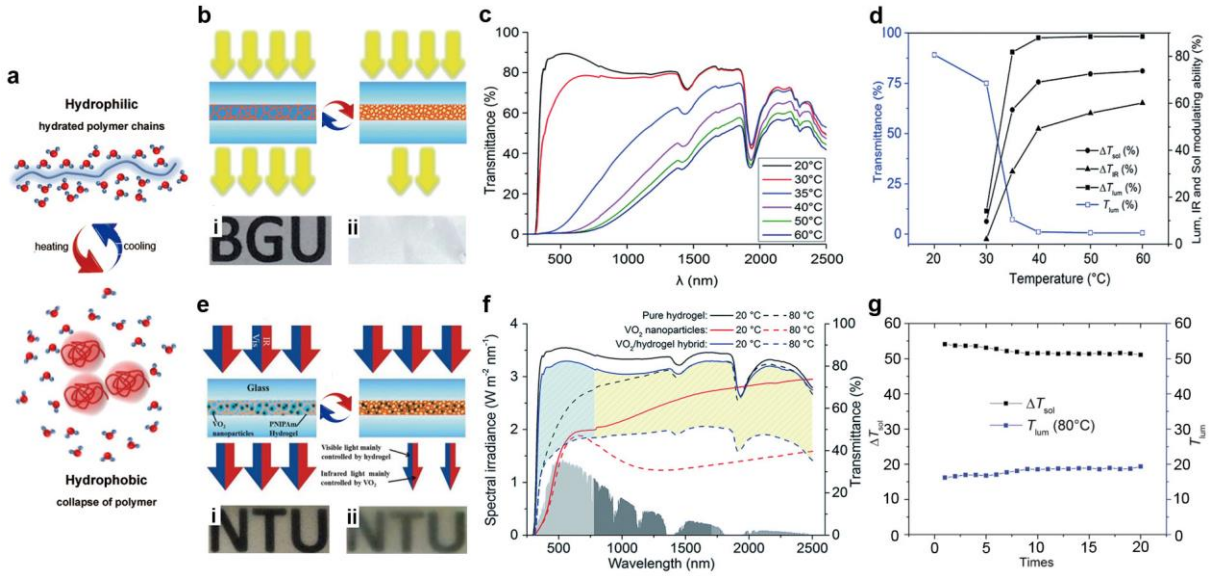

Figure 3. a) Schematic of the responsive polymer chain behavior below and above the LSCT. The top image shows the polymer chains at relatively low temperature surrounded by water molecules, and the bottom image shows the loss of water molecules and collapse of polymer chains to form polymer clusters when the temperature is elevated above the LSCT. Reproduced with permission.[21] Copyright 2016, Elsevier. b) Schematic diagram of the PNIPAm hydrogel smart window sandwich structure. The glass substrates are represented in blue and the hydrogel (red network) aggregates at elevated temperature. Incident light (golden arrows) passes through the hydrogel below 32 °C, but is largely blocked above 32 °C. The insets i and ii are the 200 μm demonstration devices at 20 and 80 °C, respectively. c) Transmittance spectrum of 200 μm PNIPAm hydrogel thin film at temperatures varying from 20 to 60 °C. d) Optical properties of integrated visible transmittance (T_{lum}), calculated solar energy modulation (ΔT_{sol}), infrared modulation (ΔT_{IR}), and integrated visible light modulation (ΔT_{lum}) of 200 μm PNIPAm film at temperatures ranging from 20 to 60 °C. Figure 3d is calculated based on the measured transmittance spectra in 3c. Reproduced with permission.[16a] Copyright 2014, Royal Society of Chemistry. e) Schematic diagram of the PNIPAm-VO_2 hybrid hydrogel smart window sandwich structure. The insets i and ii demonstrate PNIPAm-VO_2 hybrid thin films at room temperature and 35°C respectively. f) UV-Vis-NIR transmittance spectra of pure PNIPAm hydrogel, VO_2 nanoparticles and VO_2-PNIPAm hybrid hydrogel at 20 and 80 °C. g) Durability test of 100 μm PNIPAm-VO_2 hybrid film with temperature variation between 20 and 80 °C. Reproduced with permission.[16b] Copyright 2015, Royal Society of Chemistry.

2.2 Ionic liquids

Ionic liquid is defined as salt in liquid state without any decomposition or vaporization. In contrast to ordinary solvents like water, ionic liquid consists of ions and short-lived ion pairs instead of neutrally charged molecules. It has been considered the solvent of the future.[23] Paul Walden reported the first room-temperature ionic liquid in 1914;[24] since then there has

been ongoing interest in ionic liquid research and diverse potential applications have been described, including cellulose processing,[25] nuclear fuel processing,[26] solar thermal energy systems,[27] and batteries.[28]

Ionic liquid-based complex film, a mixture of transition metal compounds and ionic liquid, has received considerable attention as a promising candidate for energy-saving smart windows due to its ability to modulate solar radiation by absorption. Current research in this field is mainly focused on thermochromic ionic liquids, whose property is based on an octahedral-tetrahedral configuration change of transition metal complexes assisted by interaction with donor solvent molecules. More specifically, octahedral complexes are formed at low temperatures, while the complexes become tetrahedral at high temperatures, leading to the light transmittance variation **(Figure 4a)**.[29] The chromic variation is caused by a change in energy difference between t_{2g} and e_g orbitals through the configuration transformation:[30] in the tetrahedral configuration, the energy gap between t_{2g} and e_g orbitals is much smaller than that in the octahedral complexes; hence, resulting in a strong absorption at higher temperature and a favorable thermochromic response.

Ionic liquid-based complex materials display high sensitivity and efficiency to temperature change. For example, Wei *et al.* reported a thermochromic system of dissolved $[bmim]_2NiCl_4$ in $C_nOH_{min}^+$-based ionic liquids.[31] In this nickel(II)-based ionic liquid system, the enthalpy and entropy changes during the octahedral-tetrahedral configuration transformation were just 30-40 kJ mol^{-1} and 140-160 J $mol^{-1}K^{-1}$, respectively, leading to a promising low energy requirement that was fully achievable by exposure to sunlight. However, the solar modulation ability of pure ionic liquid-based composite systems has been insufficient for use in energy-efficient smart window applications due to the narrow modulation spectrum range. To address this issue, both inorganic and organic approaches have been developed.

The inorganic approach hybridizes an ionic liquid-based complex system with VO_2 nanoparticles. For example, Zhu *et al.* reported a composite film made up of VO_2 nanoparticles and IL-Ni-Cl complexes.[29] The pure IL-Ni-Cl displayed a significant transmittance contrast mainly in the 500-800 nm spectral range, resulting in limited modulation ability in the context of the full solar energy spectral range of 250-2500 nm **(Figure 4b)**. However, the composite of IL-Ni-Cl and VO_2 significantly broadened the modulation range and thereby promoted solar energy regulation, which was attributed to the combination of IL-Ni-Cl visible light modulation (500-800 nm) as well as VO_2 nanoparticle modulation of NIR (700-2500 nm) (**Figure 4b**). As illustrated in Figure 4b, compared with the pure IL-Ni-Cl, the VO_2 hybridized materials demonstrated significantly wider solar regulation ability covering a broad range from 500 to 2500 nm. A ΔT_{sol} up to 26.5% was achieved when such composite system was heated to 80 °C. Meanwhile, the T_{lum} at high temperature was maintained at a high level of 43.9%. A color change was observed in the composite from light brown at 20 °C to dark green at 80 °C, which was attributed to the combination of IL-Ni-Cl changing from transparent to blue whilst VO_2 remained yellow-brown **(Figure 4c)**.

A similar approach is to integrate VO_2 nanoparticles and NLETS (nickel(II)-based ligand exchange thermochromic system), which comprised nickel(II), 2,2-dimethylpropane-1,3-diol, and bromide.[32] This demonstrated a high ΔT_{sol} of 18.2% whilst maintaining a relatively high T_{lum} of 68.7% simultaneously while heated. Thus, hybridization with VO_2 nanoparticles has been recognized as a promising solution to enhance the ΔT_{sol} of ionic liquid-based complex system for energy-efficient smart windows application.

The organic approach hybridizes an ionic liquid-based complex system with thermochromic hydrogels, also known as ionogels or ion gels.[33] Besides the configuration transformation of

ionic liquid-based complex systems, an LCST-type phase transition occurs between the polymer chains and ionic liquids at elevated temperatures, leading to a remarkably distinguishable difference in optical transmittance **(Figure 4d)**. At low temperature, the polymer chains and ionic liquid form a homogeneous network that has high transparency. Upon heating, this uniform distribution of polymer chains and ionic liquid is no longer stable, resulting in the formation of ionic liquid-rich domains, scattering of incident light and a change in optical transmittance.[34] **Figure 4e** represents the transmittance spectra of ionogel at various temperatures ranging from 15 to 60 °C. With the temperature increase of ionogel, the 300-2200 nm spectral range is affected. As Lee *et al.* reported, when the ionogels were heated above the LCST, up to 80% luminous modulation (ΔT_{lum}) could be achieved via an observable color change to white (insets of Figure 4e).[35] Below the LCST, the T_{lum} was maintained at 87%. Furthermore, the exact LCST could be manipulated from below zero to over 100 °C just by varying the composition of ionic liquid. The ionogel system demonstrated high stability, maintaining solar modulation performance after 5000 heating-cooling cycles. Additionally, as shown in **Figure 4f**, this ionogel has been successfully adapted with various organic dyes, which increases its competitiveness in the commercial smart window market.

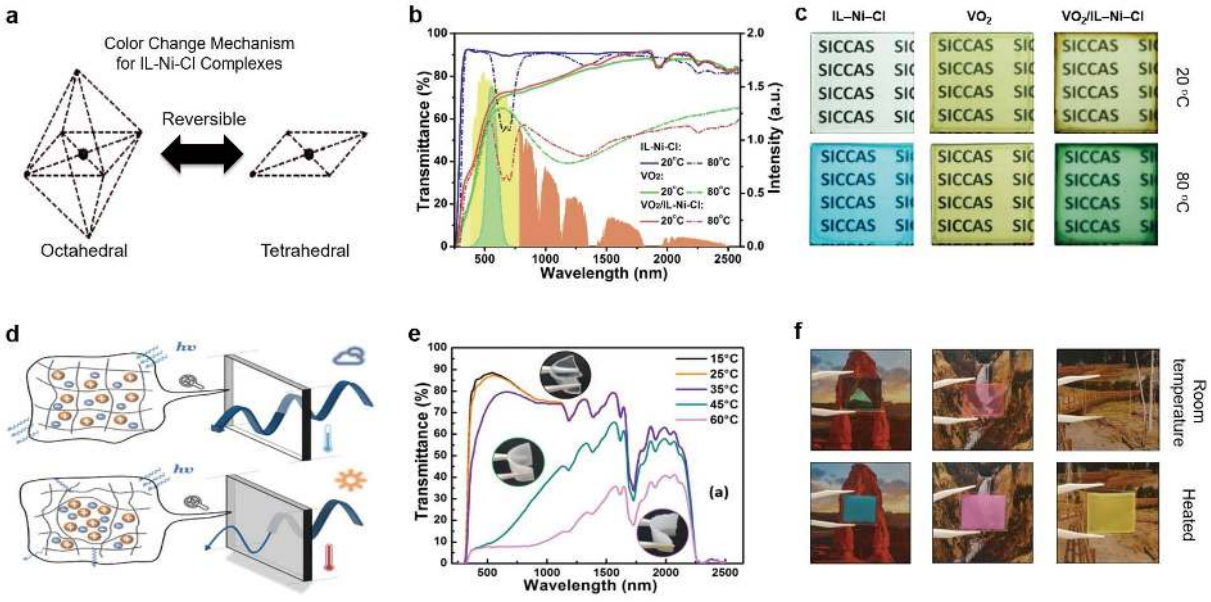

Figure 4. (a) Schematic illustration of octahedral-tetrahedral configuration change of ionic liquid-based complex system. The IL-Ni-Cl complex undergoes a phase transition from octahedral to tetrahedral above the LCST. (b) Transmittance spectrum over the UV-Vis-NIR regions of pure IL-Ni-Cl film, VO_2 nanoparticles and VO_2/IL-Ni-Cl hybrid film at 20 and 80 °C. (c) Demonstrations of pure IL-Ni-Cl film, VO_2 nanoparticle film and VO_2/IL-Ni-Cl hybrid film at 20 and 80 °C. Reproduced with permission.[29] Copyright 2016, American Chemical Society. (d) Schematic illustration of thermochromic optical transmittance change upon variation in temperature. Decreased transparency of the ionogel above the LCST results from light scattering at interfaces of ionic liquid and polymer chains. (e) Transmittance spectrum over the UV-Vis-NIR region of ionogel at various temperatures ranging from 15-60 °C. The insets are the photographs of transparent, translucent and opaque states of the ionogel, respectively. (f) Demonstration of ionogel films mixed with brilliant green, rhodamine B (RhB) and methyl orange organic dyes below and above the transition temperature, respectively. Reproduced with permission.[35] Copyright 2017, American Chemical Society.

2.3 Metamaterials

Metamaterials refer to engineered composite materials with properties that are not found in nature. These properties are not derived from the source materials themselves, but from their artificially constructed structures.[36] Various applications of metamaterials have been developed, including antennae,[37] absorbers,[38] and cloaking.[39] Metamaterials are also regarded as one competitive candidate for energy-efficient smart window applications.

In order to achieve thermal responsiveness for energy-efficient smart window applications, metamaterials could either be constructed from thermoresponsive materials,[40] or from origami-inspired metamaterials[41] attached to materials that respond to environmental temperature change, resulting in the metamaterial configuration changing spontaneously.

Whilst there appears to be great promise in the application of thermoresponsive metamaterials to energy-efficient smart window applications, this research is still in its early stage, with limited achievements to date in this field. As one category of reconfigured metamaterials, origami-inspired metamaterials have exhibited considerable potential for smart window application, with dynamically-tunable geometry of the patterned cuts and folds manipulated by external stimuli.

Tang *et al.* pioneered a thermoresponsive origami-inspired structure (also known as kirigami) that could be buckled out of plane to reflect or transmit light in response to a minor change of local temperature.[42] The so-called kiri-kirigami structure was characterized by patterned notches inserted into both sides of the sheet **(Figure 5a)**. These notches acted as geometrical imperfections of the kirigami structure, so that only certain desirable tilting orientations could be achieved. Furthermore, the tilting orientation was fully programmable by adjusting the design of notches, as demonstrated in **Figure 5b**. By integrating the thermally shrinkable tape (black) onto the patterned notches **(Figure 5c)**, a self-foldable bilayer structure formed, relying on the mismatched deformation between the thermally shrinkable tape and the kiri-kirigami metamaterial to spontaneously self-tilt upon thermal activation. Upon heating from 24 to 65 °C, the tilting orientation changed until it reversed (Figure 5c). By integration with a reflective coating, the configuration could change such that it reflected sunlight at elevated temperature and directed sunlight indoors at low temperature.

To evaluate the performance of this kiri-kirigami material, a testing space was designed with dimensions of 5200 mm (L) x 3400 mm (W) x 2300 mm (H), containing three windows, 2300 mm (L) x 580 mm (W) **(Figure 5d),** each with reflective, thermoresponsive metamaterial structure **(Figure 5e)**. **Figure 5f** shows the illumination performance of the base model without the kiri-kirigami smart windows installed, and **Figure 5g** shows the illumination performance of the proposed model with the kiri-kirigami smart windows. Taking an average day as the example, it was observed that direct penetration of sunlight decreased dramatically with the kiri-kirigami window. According to the simulation, using the kiri-kirigami smart windows throughout the year would result in a total saving of 47% and 26% electricity for cooling and lighting, respectively.

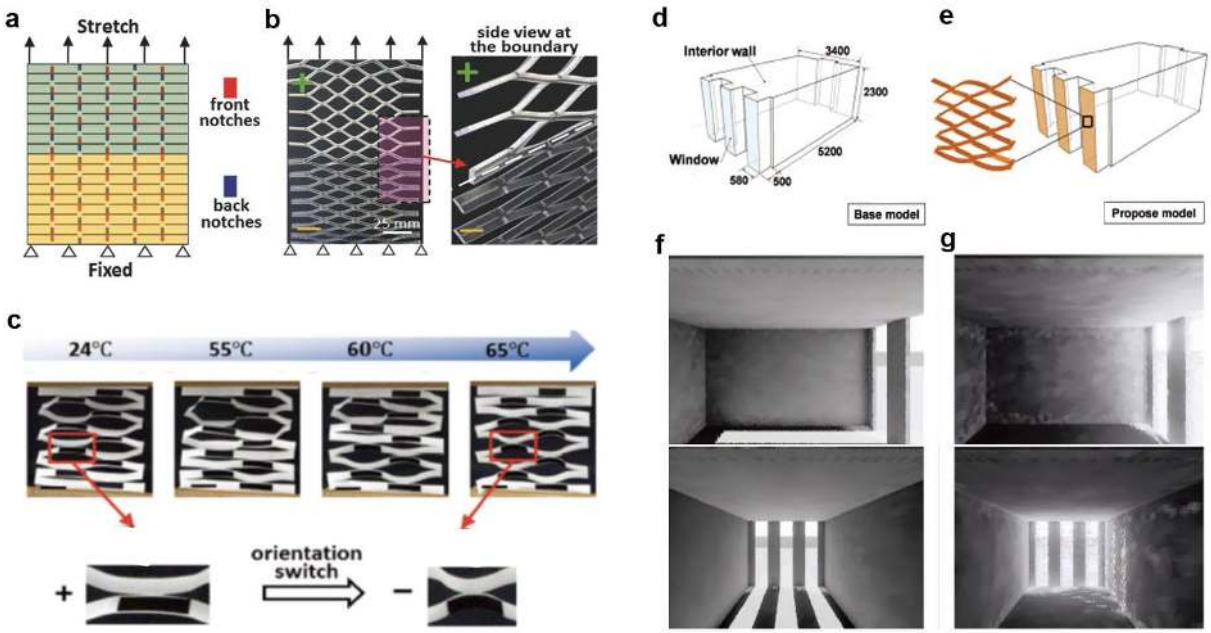

Figure 5. a) Schematic illustration of kiri-kirigami structure with notches on both sides. The upper part (green) has reversed patterned notches compared with the lower part (yellow). b) Optical images of the deformed kiri-kirigami structure with identical design to (a) upon uniaxial stretching. c) Experimental demonstrations of thermal activation and orientation switch of kiri-kirigami paper metamaterials at various temperatures. d-g) Simulation of building energy consumption while kiri-kirigami metamaterials are applied as the thermoresponsive building envelope. Schematic illustration of the stimulation space, (d) without (base model) and (e) with kiri-kirigami (proposed model) smart windows. Performance in the stimulation space of the (f) base model and (g) proposed model at noon. Reproduced with permission.[42] Copyright 2016, John Wiley & Sons.

2.4 Perovskites

Perovskites are materials with an identical crystal structure to calcium titanium oxide. Among thousands of complex structures, perovskites stand out with numerous interesting properties including chemically manipulatable optical and electrical properties.[43] There has been tremendous recent scientific interest in the development and application of perovskites, especially for photovoltaics,[44] lasers,[45] LED devices,[46] and photoelectrolysis.[47]

The general formula of perovskite is ABX_3, in which anion X is bonded to both larger cation A (positioned at cornered) and smaller cation B located at the center of the unit cell **(Figure 6a)**. For thermochromic smart window application, the thermoresponsive behavior of halide perovskites is based on their unusual crystallization behavior, also known as inverse

temperature crystallization (ITC).[48] Unlike the majority of substances, the solubility of perovskites decreases as the solution temperature increases, resulting in single crystal cell nucleation and growth of perovskite single crystals (Figure 6a). As the temperature increases, perovskite crystals gradually precipitate, accompanied by an absorbance band gap shift and optical property change.

It is the halogen constituent that determines the crystallization temperature of halide perovskites; therefore, introducing more than one halide constituent can enable further control of the thermochromic behavior of halide perovskite solutions. Pioneering work on perovskites for smart window applications was by Bastiani *et al.,* using a bi-constituent $MAPbBr_{3-x}I_x$ perovskite solution.[49] As the solution temperature was varied from 25-120 °C, the color changed from yellow to black due to the different precipitation rates of black iodine-based perovskite and orange bromide-based perovskite. The solubility of iodine-based perovskite drops much more rapidly than that of the other, therefore x increases with increasing temperature in the precipitates. Upon temperature elevation to 120 °C, the iodine-based perovskite dominated and the color turned black. During the thermochromic process of halide perovskite solution, the absorption spectrum varied significantly. The mainly absorption spectrum was 250-780 nm, which includes visible light and part of the UV region. Similar phenomena associated with halide perovskite materials have also been reported in other papers.[50] This light modulation is due to the absorption of photons by transition metal ions from the precipitate, which is affected by precipitate size and composition.[51] **Figure 6b** shows the absorption spectrum of perovskite crystals at three different temperatures. As the temperature was increased, a red-shift of the absorption edge was observed. **Figure 6c and 6d** show the thermochromic smart window prototype produced by Bastiani *et al.* and its absorption spectrum after annealing at the indicated temperature. At 60 °C, the absorption

maximum of the prototype (Figure 6d) matched well with the absorption maximum of the perovskite powder (Figure 6b). However, when the prototype was heated to 90 °C, the absorption maximum position was observed with a red-shift from 400 to 700 nm compared with 620 nm of the powder sample. Additionally, the stability of this system requires further exploration since the band edge displayed variations over several cycles of 25-60 °C heating and cooling **(Figure 6e)**. Sarkar *et al.* reported the reversible thermochromic behavior of thin film dehydrate methylammonium lead iodide.[52] With increasing temperature from 25 to 60 °C, the film demonstrated a significant absorption enhancement caused by a shift in the absorption maximum from ~400 to ~500 nm, accompanied by a distinct color variation from transparent to dark orange.

Recently, Yang *et al.* demonstrated a thermochromic smart window based on a fully reversible structural phase transitions of inorganic halide perovskite caesium lead iodide/bromide.[53] At low temperature, the non-perovskite phase with high transparency (81.7% visible transparency) is exhibited; while due to the elevated temperature, the crystals are transferred into perovskite phase, which is deeply colored with much lower transparency (35.4% visible transparency).

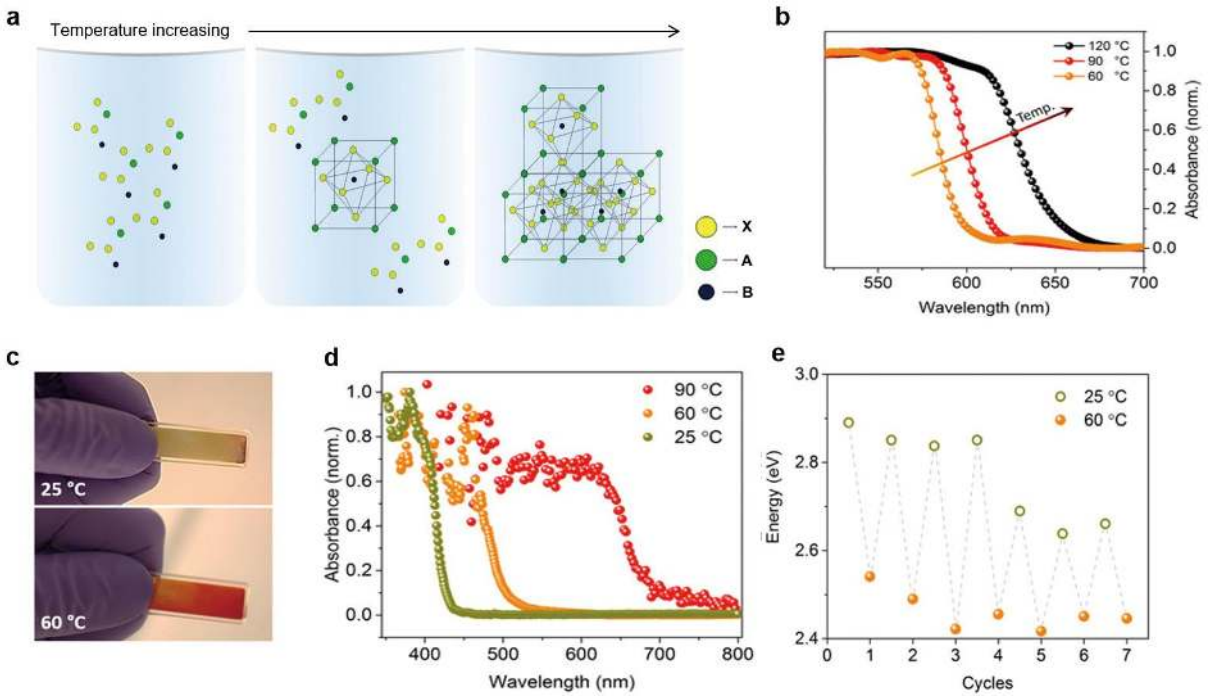

Figure 6. a) Schematic illustration of the inverse temperature crystallization (ITC) process of perovskite materials: with increasing temperature, the perovskite crystals nucleate and grow. b) Absorption spectra of perovskite crystals obtained from inks at 60, 90 and 120 °C. c) Photographs of thermochromic prototype annealed at 25 °C (top) and 60 °C (bottom). d) Absorption spectra of the thermochromic prototype after annealing at the indicated temperature. e) Band edge alternation of the thermochromic prototype during heating and cooling cycles between 25 and 60 °C. The green circles represent the extrapolated maxima at 25 °C; the red spots represent the extrapolated minima at 60 °C. Reproduced with permission.[49] Copyright 2017, American Chemical Society.

2.5 Liquid crystals

Liquid crystals (LCs) represent the a new class of material, which is intermediate between the conventional liquid and crystalline solids and may flow like a liquid while the molecules are well-oriented in a crystal-like way.[54] Most liquid crystals are made of organic compounds. They are characterized by the anisotropy of optical, electrical, and mechanical properties.[55] These properties are responsive to a variety of stimuli, including the temperature, electric field, light etc., which make LCs broad interesting in applications.[56]

Optical properties of LCs highly rely on the orientation of anisotropic molecules. The thermochromism of LCs is achieved by tuning the orientation in response to temperature stimulus.[57] In a sandwich configuration smart window, LC molecules can be tuned in a

number of orientation between two glass slides. **Figure 7a** shows three typical orientations of LCs and the corresponding optical states that affect the incident light perpendicular to the glass slide. When the molecules are assembled in helical structures and parallel to the slides (planar orientation), the incident light is reflected (reflective state). A light scattering state form when the helical structures are randomly tilted in a focal conic orientation. The LCs perform to be transparent when the molecules extend perpendicular to the slides (homeotropic alignment). In scattering and reflective states, the reflection band is determined by incident angle of light, the pitch of LCs, and the refractive index of materials.

Thermochromic films based on orientation transition of LCs have been demonstrated as a good candidate for energy-efficient smart windows. Akifumi *et al.* reported the thermal-induced transmittance-to-diffraction states of holographic polymer-LC composite.[58] The group of Yang has produced a series of thermochromic films based on the polymer-LCs composites. In these works, the LCs represented a light modulation in a broadband (400-2500 nm) with strong control in visible range. They prepared a thermochromic film based on a polymer stabilized LC, while the planar orientation of LC molecules at low temperature gave low solar energy transmittance, which is not desired. [59] Later, they produced a coexistent system containing polymer-stabilized and polymer-dispersed LCs. [60] Films based on the system were observed a higher transparency at low temperature and a narrow thermal hysteresis (less than 2 K) in 42 ^{o}C. To further decrease the NIR irradiation, they introduced the inorganic nanocrystals (NCs) with strong NIR absorption, such as ITO[61] and $CSxWO_3$,[62] to the polymer-LC composite. For example, they developed a dual-response film containing well-dispersed ITO NCs and LC droplets in phase-separated polymer network **(Figure 7b)**. [61] The LC could be changed reversibly from focal conic to homeotropic orientations by either thermal or electrical field stimuli **(Figure 7b1)**. In this case, the

transition here was also suggested as a smectric (SmA) to chiral nematic (N*) phase transition. The film was observed changes from opaque to transparent appearances during the transition **(Figure 7b2)**. On the film with 5 wt% ITO, it was demonstrated with a low NIR transmittance (~15%) from 1400 to 2500 nm as well as a huge transmittance contrast at 400 nm up to ~70% between at 300 and 308 K **(Figure 7c)**. The introduction of ITO NCs also slightly decreased the transition temperature **(Figure 7d)**, which was explained as the effect of ITO NCs residue in the LC domain after phase transition. It is worthy to mention that these films are easily processable and were successfully produced in meter scale by a roll-to-roll method **(inset of Figure 7c)**.

Hybrid film was studied by Liang et al. by combining the electrochromic LC with the thermochromic VO_2. [63] In the experiment, W-doped VO_2 (W-VO_2) NCs and LCs were homogeneously dispersed in the phase-separated polymer framework **(Figure 7e1)**. The electrochromics of LCs and thermochromics of W-VO_2 NCs were maintained after combination and could work independently, which made the stimulus-responsive film display four optical states under different stimuli: low temperature/no electrical field, high temperature/no electrical field, low temperature/electrical field, and high temperature/electrical field **(Figure 7e2)**. For example, the film with 2.5 wt% W-VO_2 displayed decreasing transmittance in NIR spectrum range under increasing temperature from 25 to 55 ^{o}C **(Figure 7f)**. The transmittance (400-2500 nm) was further decreased by increasing the applied voltage from 0 to 35 V with a significant depression in visible range **(Figure 7g)**. The optimized ΔT_{sol} was achieved up to 34.6%, which is comparable to the hydrogel/VO_2 hybrid.

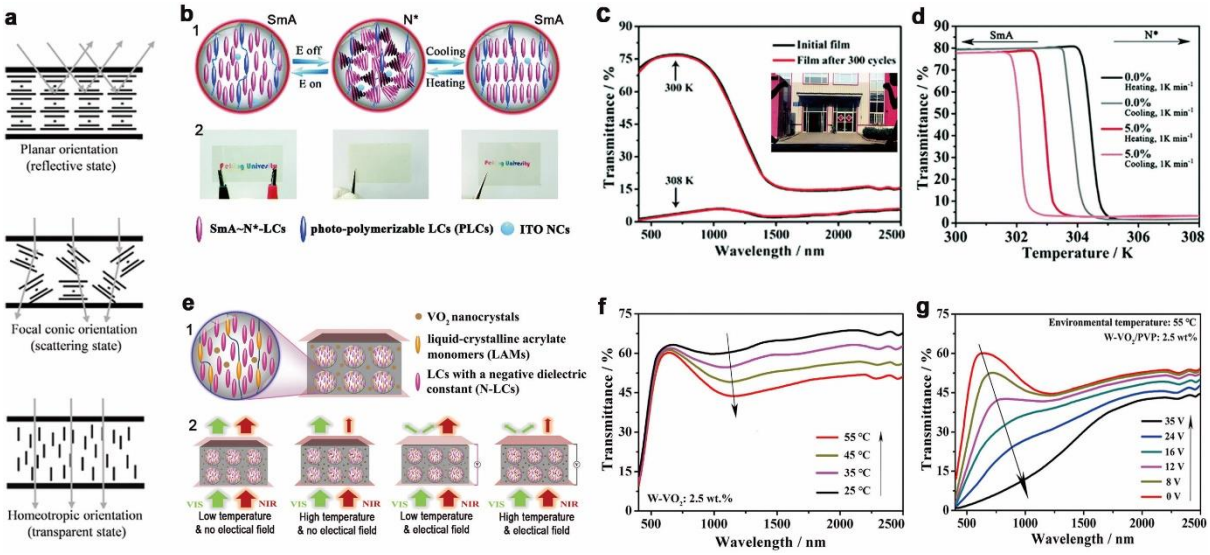

Figure 7. a) Schematic of the orientation-dependent optical behavior of cholesteric liquid crystalline materials. Reproduced with permission. [57] Copyright 2017, John Wiley & Sons. b) Schematic of the smectic A (SmA) to chiral nematic (N*) phase transition in a cell containing the liquid crystals (LCs) and indium tin oxide (ITO) nanocrystals (NCs). The transition can be reversibly induced by either electric- or thermal-stimulus (b1), accompanying with distinct transparency change, demonstrated as the corresponding photographs (b2). c) Temperature-dependent transmittance spectra of the smart film consisting 5 wt% ITO NCs before and after 300 cycles. Inset of (c) is the photography of the meter-scale film. d) Temperature-resolved transmittance at 560 nm of smart films containing 0% and 5 wt% ITO NCs. Reproduced with permission. [61] Copyright 2017, Royal Society of Chemistry. e) Schematic of the VO_2-LCs composite film (e1) with four optical states under different stimuli (e2). f) Temperature-dependent spectra of the composite film containing 2.5 wt% W-doped VO_2. g) Electric-field-dependent of the transmittance spectra of the composite film containing 2.5wt% W-doped VO_2 at 55 °C. Reproduced with permission. [63] Copyright 2017, Royal Society of Chemistry.

2.6 Discussion and comparison to VO_2

Considering the huge potential impact of emerging materials on the traditional VO_2 in thermochromic smart window applications, it is of great interest to compare emerging thermoresponsive materials to the conventional VO_2 material.[8, 9b] This section begins with a brief introduction to VO_2, followed by a comparative discussion on the advantages and disadvantages of each material in terms of ΔT_{sol}, T_{lum}, , transition temperature, and durability.

VO_2 undergoes a reversible monoclinic to rutile crystal transition at the τ_c of 68 °C.[64] Below τ_c, VO_2 displays a distorted rutile structure, characterized as atomic zigzag chains consisting

of vanadium ions with interlaced V-V distances of 3.19 and 2.60 Å. Above τ_c, it presents a tetragonal rutile phase with V^{4+} ions at the corner and center positions with a V-V distance of 2.85 Å along the c-axis **(Figure 8a)**.[64a] The transition induces an abrupt optical transmittance change mainly in the IR spectral range, which has made VO_2 attractive for smart window applications.[65] Another important advantage of pure VO_2-based thermochromic film is that it works "silently":[66] compared to the pronounced color changes of most electrochromic and photochromic smart windows,[67] The color, transparency and T_{lum} remains constant due to its negligible variation in the visible range in response to temperature. Nevertheless, there remain intrinsic shortfalls of VO_2 that hamper its practical applications. The following section is to compare the pros and cons of emerging thermoresponsive materials with VO_2.

Firstly, the pure VO_2 system displays a limited ΔT_{sol} that is commonly lower than 20% with an acceptable T_{lum} of 50%. [7a] This is largely attributed to the negligible optical modulations in the visible range, where nearly half of solar energy exists **(Figure 8b)**. However, emerging materials such as hydrogels display excellent control within both the NIR and visible ranges (Figure 8b), giving to significantly enhanced performance in solar energy regulation. For example, PINIPAm-based thermochromic films were demonstrated to have an optimized ΔT_{sol} of ~26% upon a T_{lum} above 70%,[16a] which surpassed the best reported VO_2-based thermochromic films, including those produced with controlled porosity,[68] nanothermochromism,[69] moth-eyed nanostructure, antireflective overcoating,[70] as well as doping[71] and nanogriding methods **(Figure 8c)**.[72] The hybrid combining VO_2 and PNIPAm also displayed a high level of performance that could not be achieved by the pure VO_2 system (Figure 8c).[16b] Thermochromic perovskite and reconfigured metamaterials have also demonstrated visible light control but the quantitative optical calculations are missing and

more researches are needed in those two categories. It is reasonable to consider these materials as promising candidates for solar energy modulation.

Secondly, accurate control to tune the optical intensity in specific spectral ranges is a desirable approach in thermochromic smart window materials due to the nonuniform distribution of the solar spectral irradiance (Figure 8b). Recent research on VO_2 has achieved precise control, wherein a size-controlled preparation method for patterned VO_2 nanoparticles was achieved using a sacrificial colloidal template **(Figure 8d)**.[5c] An emerging extinction peak was observed upon increasing temperature **(Figure 8e)**, known to be the localized surface plasmon resonance (LSPR) that occurs on particles with constrained size on the nanoscale (commonly less than 100 nm).[73] The position of the LSPR could be tuned from 1120-1360 nm by controlling the particle size and the reflective index of the medium **(Figure 8f)**. This work indicates the possibility of promoting solar modulation efficiency by tuning the absorption position to the range with densest solar energy. Compared with the well-studied VO_2, emerging materials have displayed a lower degree of controllability in terms of the position and intensity of the responsive spectral range. For example, the PNIPAm hydrogel blocked a broad spectral range of 250-2500 nm, leading to white opaque appearance while the transparency is needed in many glass applications.[16a] This issue may be tackled if the size and arrangement of polymer clusters could be controlled to selectively scatter the incident light in a narrow spectral range.

Thirdly, the transition temperature range of emerging thermoresponsive materials is suitable and easily processable. The τ_c (68 °C) of typical VO_2 is too high for smart window applications. Although methods such as doping can reduce the τ_c, these methods are commonly achieved *via* crystallographic engineering and are accompanied by some sacrifice of thermochromic properties. [74] On the other hand, all the reported hydrogels,

thermoresponsive perovskites, reconfigured metamaterials, and liquid crystals show suitable transition temperatures, starting from 25 °C. In addition, their different transition mechanisms offer more freedom to modify their transition temperatures with the potential not to jeopardize their optical performance. For example, the heat-shrinkable tapes determine the transition temperature range while contributing little to the optical properties of programmable kiri-kirigami metamaterials.[42] These tapes can be changed according to specific circumstances.

Finally, durability must also be considered in real applications. A challenge of VO_2 is its weak resistance to oxidization,[5b, 75] and emerging thermoresponsive materials have not yet demonstrated sufficient durability. For example, thermoresponsive perovskite displayed an obvious band gap variation within less than 10 heating-cooling cycles.[49] Although a few emerging thermoresponsive materials studies have considered their durability, these tests were far from adequate for real applications. It is believed that improvements to prolong durability are necessary for all these emerging thermoresponsive materials.

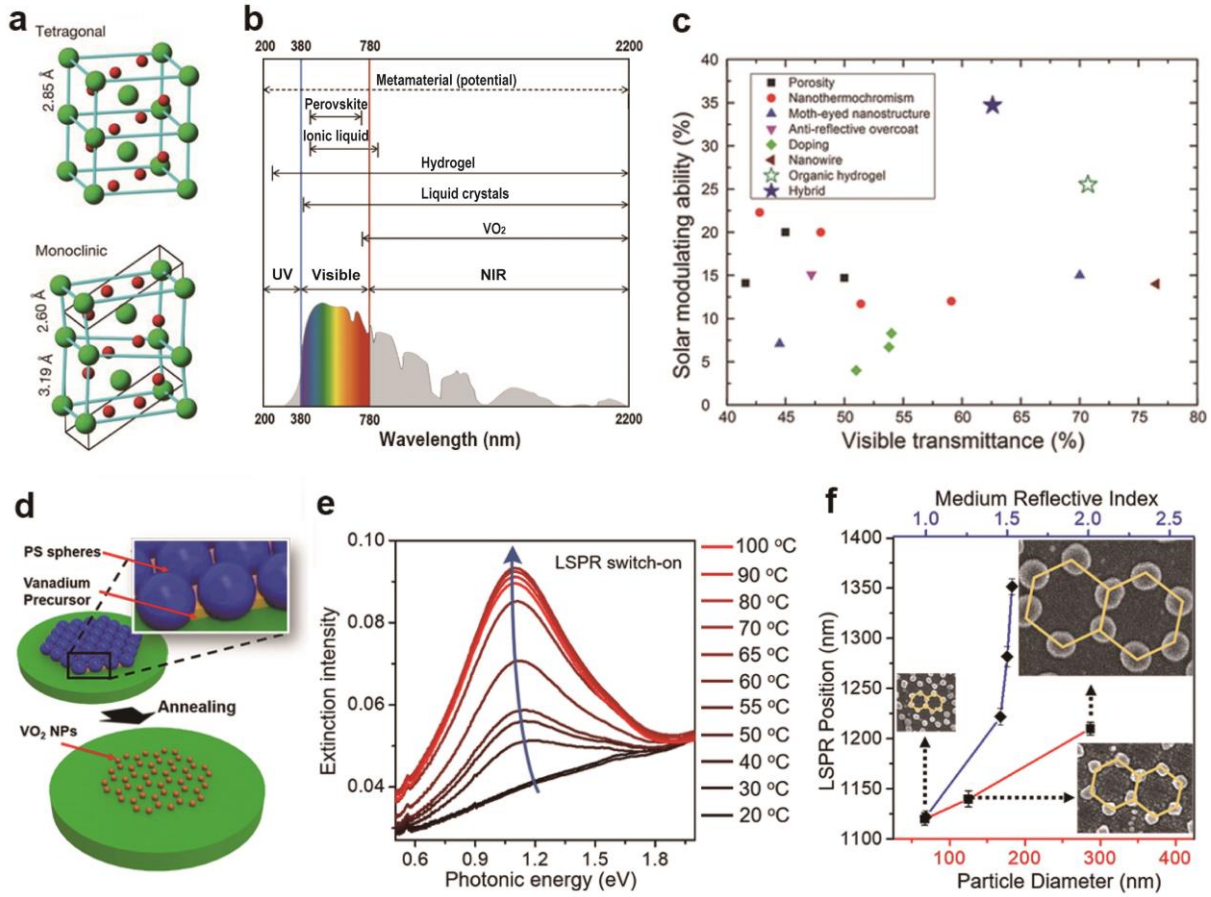

Figure 8. a) Crystal structures of tetragonal (top) and monoclinic (bottom) VO_2. b) Summary of the spectral ranges that can be modulated by metamaterials, perovskites, ionic liquids, hydrogels, liquid crystals, and VO_2. Reproduced with permission.[76] Copyright 2014, Nature Publishing Group. For the metamaterials, the potential spectral range is indicated since accurate data is not available. c) Summary of quality data on solar energy modulation ability (ΔT_{sol}) and visible transmittance reported for methods including porosity, nanotherchromism, moth-eye nanostructure, anti-reflective overcoat, doping, nanowire, organic hydrogel, and VO_2/hydrogel hybrid. Reproduced with permission.[77] Copyright 2016, John Wiley & Sons. d) Illustration of the preparation method of VO_2 nanoparticles (NPs) through the sacrificial two-dimensional colloidal templates made by polystyrene (PS) spheres. e) The temperature-dependent extinction of hexagonal patterned VO_2 NPs with an average diameter of 67 nm. The localized surface plasmon resonance (LSPR) rises upon increasing temperature. f) The LSPR position of hexagonal patterned VO_2 NPs in relation to particle diameter and medium reflective index. Insets are scanning electron microscopy (SEM) images of patterned VO_2 NPs with average diameters of 67, 125, and 287 nm. Reproduced with permission.[5c] Copyright 2017, American Chemical Society.

3. Integrated techniques

3.1 Self-cleaning and wettability

Water and adhering pollutants contact windows in daily life, which may lower their transparency, increase cleaning cost, and reduce aesthetic appeal. To address these problems, there has been increasing scientific attention on multifunctional energy-efficient smart windows, such as by integration with the wettability and self-cleaning property.[78] Application of highly transparent coatings onto the functional energy-saving layer has been demonstrated to be a simple but highly effective method. Both inorganic and organic coatings have been developed, with most studies on a VO_2-based energy-saving layer.

An attractive inorganic coating is TiO_2(A) (anatase) due to its effective photocatalytic degradation of organic contaminants, antireflection properties when coated on a VO_2 surface, and high transparency in the visible range.[79] For example, Parkin's group produced a $TiO_2/SiO_2/VO_2$ multilayer for the bifunctionality of self-cleaning and energy saving **(Figure 9a)**.[80] Under UV illumination (I=4 mW cm^{-2}), the TiO_2(A)-coated sample was observed to effectively remove adherent stearic acid over time, which was comparable to the performance of commercial Pilkington Activ glass **(Figure 9b)**. The self-cleaning character of TiO_2(A) arises from its photocatalytic property, as indicated by comparison of the molecular quantity of degraded stearic acid per incident photon (ξ) on these four samples **(Figure 9c)**. The sandwiched SiO_2 layer acts as a barrier to diffusion of Ti^{4+} ions as well as to enhance antireflection performance.

SiO_2 coatings and shells on VO_2 have been widely studied due to their inert properties.[74b, 81] In one study, instead of applying a sandwiched SiO_2 layer, TiO_2(A) and TiO_2(R) were directly deposited on each side of a planar VO_2 layer **(Figure 9d)**.[82] The film wettability changed from hydrophobic (contact angle of 86.4°) to hydrophilic (contact angle of 3.7°) with increasing UV illumination duration **(Figure 9e)**. It was suggested that this wettability change was attributed to both the removal of adsorbents under longer exposure and the gradual

stoichiometry change of VO_2. There was also a gradual decrease in the absorbance signal of rhodamine B (RhB) on the TiO_2(R) surface, which demonstrated the contaminant removal behavior of the TiO_2(A)/VO_2/TiO_2(R) multilayer potentially suitable for smart window application **(Figure 9f)**. Furthermore, the coating of ZnO on VO_2 has also been found to impart enhanced durability, antibacterial and biocompatible properties.[81, 83]

Thin organic coatings are another good candidate for providing tunable wettability whilst maintaining sufficiently high transparency for solar energy modulation. Flourooctyl triethoxysilane (FOS) was demonstrated to be a good candidate.[84] Qian *et al.* coated a thin layer of FOS on VO_2/SiO_2 nipple arrays to impart hydrophobicity to the thermochromic film.[72b] In a biomimetic moth-eye structure, 40 nm thick VO_2 was coated onto the nipple array nanostructured SiO_2 substrate with a periodicity of ~210 nm **(Figure 9g)**. The optical properties and wettability of the 210 nm-patterned VO_2 was investigated before and after application of a thin FOS coating, with the measured transmittance spectra indicated as the red and green lines, respectively, on the left in Figure 9h. It was found that application of the FOS coating caused a negligible transmittance decrease in the visible spectrum, while the contact angle changed from 58 to 118° (right hand images in **Figure 9h**). Besides the surface chemical modification, the nipple array VO_2 displayed a larger contact angle than that of the planar VO_2 (26 °C), which was attributed to roughness-enhanced wettability in accordance with the Wenzl model.[85] This surface morphology, which induced the wettability enhancement, was also applied in several applications relating to energy-saving glazing using rough VO_2 or its composite with polymethylmethacrylate (PMMA).[86]

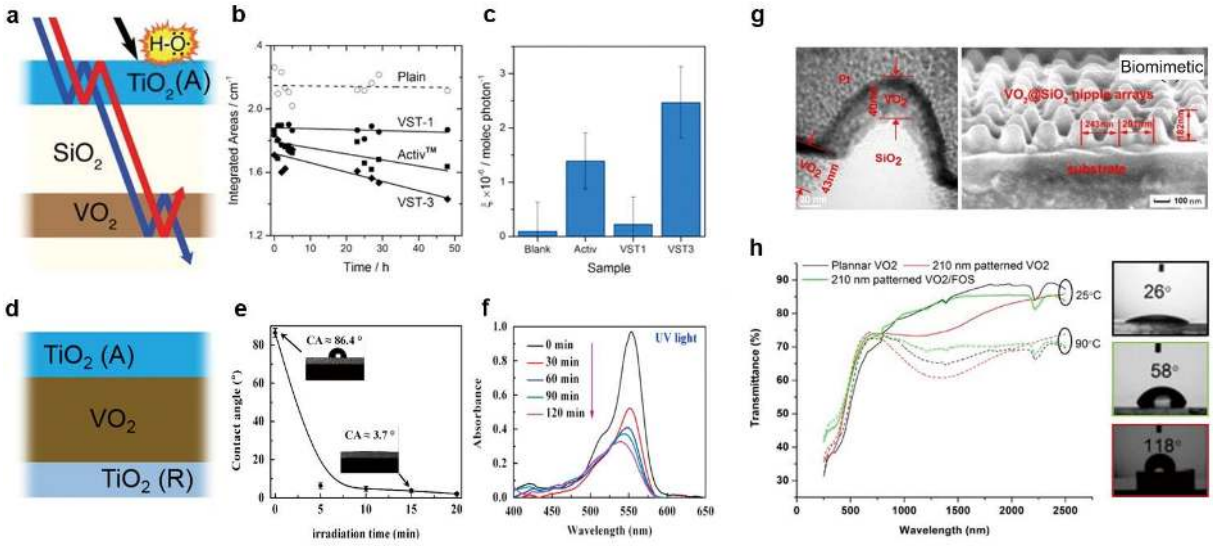

Figure 9. a) Illustration of the $VO_2/SiO_2/TiO_2$(A) multilayer for self-cleaning and energy-saving coatings. b) and c) Degradation of stearic acid under UV illumination (I=4 mW cm^{-2}) on $VO_2/SiO_2/TiO_2$(R) (VST-1), $VO_2/SiO_2/TiO_2$(A) (VST-3), plain (blank), and Pilkington Activ glass (Activ): b) Time-dependent integrated area of stearic acid; c) The calculated corresponding formal quantum efficiency (ξ), presenting the molecular quantity of degraded stearic acid per incident photon. Reproduced with permission.[80] Copyright 2014, American Chemical Society. d) Illustration of the TiO_2(A)/VO_2/TiO_2(R) multilayer. e) Time-resolved contact angle change on the TiO_2(A) surface with hydrocarbon adsorbates. f) Absorbance spectra of rhodamine B (RhB) on the TiO_2(A) surface under a constant UV light irradiation with increasing time. Reproduced with permission.[82] Copyright 2015, Elsevier. g) TEM image of an individual VO_2-coated SiO_2 nipple nanostructure (left) and SEM image of the nipple array with 210 nm periodicity (right). h) Transmittance spectra at 25 and 90 °C (left) as well as contact angle measurements (right) of planar VO_2, 210 nm-patterned VO_2 and 210 nm-patterned VO_2/FOS. Reproduce with permission.[70b] Copyright 2014, American Chemical Society.

3.2 Integration with solar cells

Combining energy conservation and generation into one device is a highly attractive scientific undertaking. Smart windows with both of these properties have been achieved by either integrating solar cells (SCs) with VO_2-based thermochromic layers or relying on thermochrmic perovskite materials.[87]

One approach utilized the light scattering induced by the VO_2 nanoparticles.[87a] In this method, the solar cell was attached to the sides of the VO_2-based thermochromic film, which consisted of a VO_2@SiO_2@TiO_2 nanoparticle/polyurethane (PU) composite layer between

two light guide layers (LGLs) **(Figure 10a)**. The incident light was scattered by the VO_2@SiO_2@TiO_2 nanoparticles to the adjacent SCs, facilitating electricity generation (Figure 10a). A ΔT_{sol} of 7.5% accompanied by a power conversion efficiency of 0.52% was achieved. Another approach was to use the light transmitted through VO_2-based thermochromic film.[87b] **Figure 10b** represents the layered configuration, which sequentially consisted of VO_2 thermochromic film, Ag nanowires (AgNWs), ZnO, a photoactive layer, poly(3,4-ethylenedioxythiophene):polystyrene sulfonate (PEDOT:PSS), and an indium tin oxide (ITO) layer. The photoactive layer is consisted of the diketopyrrolopyrrole-quinquethiophene alternating copolymer:[6,6]-phenyl-C_{60}-butyric acid methyl ester (pDPP5T-2:PC_{60}BM). The VO_2-based thermochromic film was made of VO_2 nanoparticles and polyvinyl pyrrolidone (PVP) composite. Distinct layer boundaries were observed using SEM **(Figure 10c)**. Compared to the performance of the scattering-based approach, the power conversion efficiency was significantly improved to 3.1%, whilst maintaining the same ΔT_{sol} of 7.5%. However, the T_{lum} of both configurations decreased considerably to of 28.2%. Further research efforts are necessary to enhance the energy conservation and generation performance of integrated smart windows.

More recently, Yang et al. reported a bi-functional thermochromic halide perovskite based solar cell.[53] While the temperature is low, the device is transparent with low power output. Whereas, transparency drops significantly while the critical phase transition temperature of 105 ^{0}C is reached. At the deeply colored state, the device can not only block the solar radiation, but also absorb the solar light and generate electricity with peak efficiency above 7%. Additionally, the device demonstrates acceptable stability and reversibility over the repeated phase transition cycles without color fade or performance degradation.

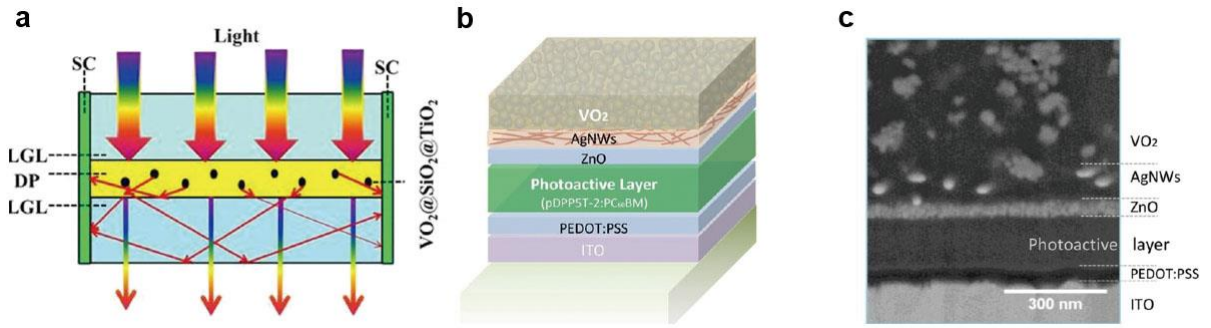

Figure 10. a) Illustration of the integrated SC and VO_2-based thermochromic film utilizing light scattering. The light guide layer (LGL) and the low reflective index medium (DP) are made of polycarbonate (PC) and VO_2/polyurethane (PU) composite, respectively. Some of the incident light is scattered to the SCs. Reproduced with permission.[87a] Copyright 2013, Nature Publishing Group. b) Illustration of the layered integration of SC and VO_2-based thermochromic films utilizing light transmittance. pDPP5T-2:PC_{60}BM and PEDOT:PSS refer to the diketopyrrolopyrrole-quinquethiophene alternating copolymer:[6,6]-phenyl-C_{60}-butyric acid methyl ester and poly(3,4-ethylenedioxythiophene):polystyrene sulfonate, respectively. c) The cross sectional SEM image of the multilayer configuration corresponding to the illustration of (b). Reproduced with permission. Copyright 2015,[87b] John Wiley & Sons.

3.3 Electro-thermal technique

Temperature-sensitive smart windows are commonly considered to be a passive energy conservation device because they respond to surrounding temperature automatically. Integration of electro-thermal techniques with thermoresponsive materials brings so-called "active control" to temperature-sensitive smart windows (as well as to other thermochromic devices). Recent studies have focused on developing electrically-controlled devices by superimposing different transparent electrodes onto the temperature-sensitive layers, which have been composed of VO_2- and hydrogel-based films. The working mechanism of the electro-thermochromic system is simple: joule heating upon an applied voltage to the transparent electrodes.

As a conventional thermochromic material, VO_2 crystals have been investigated in combination with various conductive substrates for electro-thermochromic devices. The VO_2 nanoparticles were deposited on the substrate with transparent electrodes, such as Ag nanowires or ITO glasses.[88] When sufficient voltage was applied across the electrode, joule

heat was generated and transferred to the VO_2 crystals; when the τ_c was reached, solar transmittance variation occurred due to a metal-insulator phase transition. Furthermore, the solar modulation performance of the electro-thermochromic system, especially in the infrared region, could be dynamically manipulated according to the applied voltage with excellent reversibility and stability. A double-layered VO_2-based structure and its fabrication process reported by Li *et al.* is illustrated in **Figure 11a.**[89] In the VO_2/Ag NW system, the solar transmittance of the VO_2 based electro-thermochromic system in the NIR region decreased gradually as the applied voltage was increased from 0 to 6 V, and a significant drop of transmittance at 1200 nm from ~70% to ~30% was observed as the applied voltage was further increased to 6.5 V **(Figure 11b)**. The solar modulation performance was also dependent on the thickness of the VO_2 nanoparticle film: thick film resulted in better performance. **Figure 11c and 11d** show the transmittance hysteresis loop of the VO_2 based electro-thermochromic system as a function of applied voltage at 1.5 μm, and the infrared response at 1.5 μm, respectively, which indicated high reversibility and stability. In an additional approach, VO_2 was hybridized with liquid crystals for smart window applications.[63] The hybrid displayed independent responses to voltage and heat stimuli. Chen *et al.* reported another approach using monoclinic crystalline muscovite mica as the substrate.[90] The VO_2-film was prepared using rf-plasma-assisted oxide molecular beam epitaxy (MBE), and a layered, single-walled carbon nanotube film deposited by the chemical vapor method was employed as the electrode.

Electro-thermochromic devices have also been developed based on thermochromic hydrogels. For example, Zhou *et al.* reported a PNIPAm-based electro-thermochromic system composed of silver nanoparticle transparent electrodes, assembled into either a regular or honeycomb shape grids **(Figure 11e)**.[77] When applied to smart window applications, it was found that

the solar modulation performance of the electro-thermochromic system was not only dependent on the external voltage applied but also on the structure of silver grids on the transparent electrodes. As the structure changed from square to honeycomb, solar transmittance dropped significantly across the UV-Vis-NIR region **(Figure 11f)**. The response time, which is the time required for the hydrogel electro-thermochromic system to transform from water-clear to paper-opaque, decreased with increasing voltage applied. When the applied voltage was increased from 2, to 4, to 6 V, the response time dropped from 120, to 70, to 40 s, respectively **(Figure 11g)**. A demonstration of this hydrogel-based electro-thermochromic system is shown in **Figure 11h**. The hydrogel film becomes opaque in only a few seconds with a steady current of 0.6 A applied. Kiruthika *et al.* have reported a hydrogel-based electro-thermochromic system made up of hydroxypropyl methyl cellulose (HPMC) and Sn wire network.[91] An transmittance contrast of over 60% across the UV-Vis-NIR region was observed before and after the voltage was applied. The energy consumption of this device was as low as 0.2 W/cm^2. Additionally, to resolve the cost issue of conventional silver nanowires or ITO materials, Sn mesh electrodes and Cu mesh electrodes were developed by Kiruthika *et al.* and Singh *et al.,* respectively, which also improved the commercial compatibility of the electro-thermal system.[91,92]

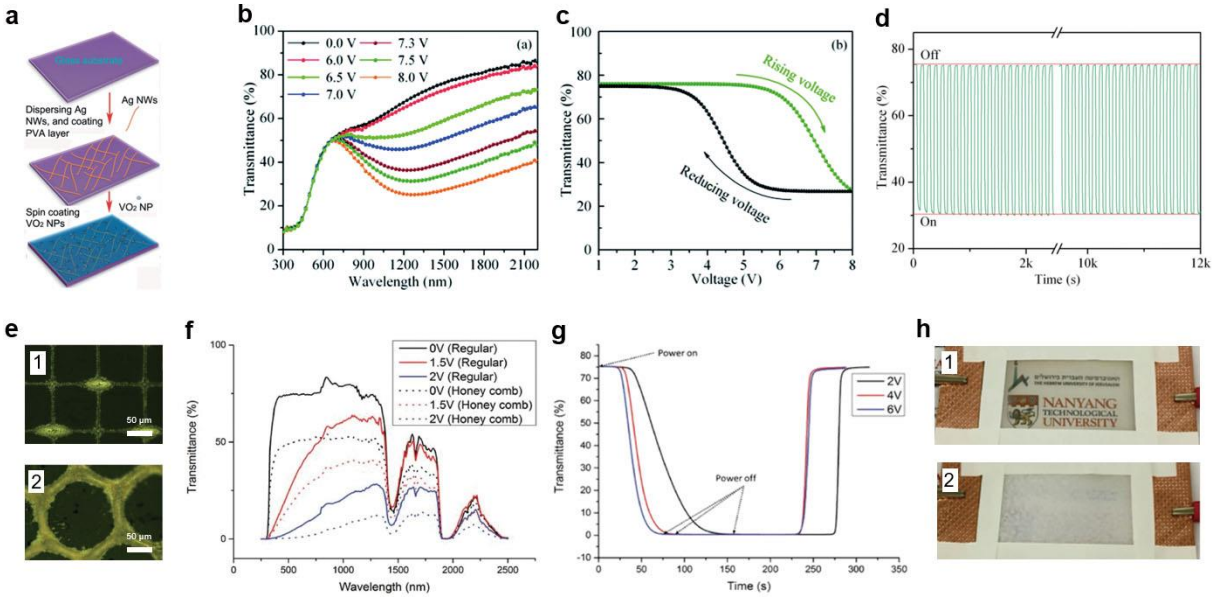

Figure 11. a) Schematic representation of a VO_2/Ag-based electro-thermochromic device and its fabrication process. Firstly, Ag nanowires are deposited on the pre-cleaned glass substrate, followed by a thin layer of polyvinyl alcohol (PVA). The VO_2 nanoparticles are deposited on top of the PVA film by spin coating. b) UV-Vis-NIR transmittance spectrum of the VO_2/Ag based electro-thermochromic device at various voltages from 0 to 8 V. c) Transmittance hysteresis loop of the VO_2/Ag-based electro-thermochromic device as a function of applied voltage at a wavelength of 1.5 μm. d) Infrared response of the VO_2/Ag based electro-thermochromic device with 8 V applied voltage at 1.5 μm. Reproduced with permission.[89] Copyright 2014, Royal Society of Chemistry. e) Optical microscope images of self-assembled electrodes in (1) square and (2) honeycomb shapes. f) Transmittance spectra of hydrogel-based electro-thermochromic devices with different electrode alignments at 0-2 V applied voltage. g) Response time of square shaped hydrogel-based electro-thermochromic device with 2-6 V applied voltage. h) Demonstration of hydrogel-based electro-thermochromic device (1) with and (2) without voltage applied. Reproduced with permission.[77] Copyright 2016, John Wiley & Sons.

4. Conclusion and perspective

In conclusion, the rapid development of energy-efficient smart windows has attracted increasing research interest in the exploration of novel thermoresponsive materials and related integrated techniques. Emerging materials including hydrogels, ionic liquids, perovskites, metamaterials, and liquid crystals have been systematically summarized and compared with VO_2, a conventional material for thermochromic smart window applications. In addition, progress of integrated techniques including electro-thermal, self-cleaning, wettability, and integration with solar cells has been discussed.

Challenges and opportunities remain in the future development of the smart architectural window, with the aim of achieving high energy-saving efficiency. We summarize the achievement and discuss remaining challenges by catagories as in Table 1. Moreover, we suggest the general guideline for future development from both the material and integration technique sides.

Table 1. Summary of achievements and remaining challenges by categories.

Category		Achievement			Reference	Challenge
		Modulated solar spectrum (250-2200 nm) / nm	Transition temperatures / °C	Appearance changes during transitions		
Thermal-responsive materials	Hydrogels	250-2200	32	Transparent-to-white	[15-17], [77]	Liquid phase that requires rigorous encapsulation
	Ionic liquid	500-800	\	Transparent-to-colorful	[29], [32], [35]	Liquid phase that requires rigorous encapsulation and a narrow spectrum of solar modulation
	Metamaterials	200-2200	55-65	\	[42]	For kirigami-based metamaterials, hollow space is essential for operation and facile fabrication of structure in small scale (less observable) are preferable
	Perovskites	400-700	25-90	Colorful-to-colorful	[49], [52,53]	Liquid phase that requires rigorous encapsulation, the stability improvement is necessary, and a narrow spectrum of solar modulation
	Liquid crystals	400-2200	29-33	Transparent-to-white	[58-63]	Liquid phase of scattering state (chiral nematic, N*, phase) that requires rigorous encapsulation
Integrated techniques	Self-cleaning and wettability	These could be achieved by either inorganic, organic coatings or the surface morphology modification.			[70b], [79-84], [86]	Reducing the visible transmittance and solar energy modulation performance in most cases
	Integration with solar cells	These could be achieved by either integrating with photoactive layers or using thermochromic perovskites			[53], [87]	Limited energy-saving property with relative low energy generation performance
	Electro-thermal technique	These could be achieved by transparent electrodes consisted of ITO, Ag NWs, carbon nanotube, Sn, or Cu.			[63], [77], [88-92]	Extra energy consumption is required. The technique reduces the visible transmittance and solar energy modulation performance in most cases

Note: "\" means data not available.

On the materials side, it is worthwhile to explore novel thermoresponsive materials as well as to further optimize the properties of current materials. Considering the expansive range of thermoresponsive materials,[93] the exploration of new materials and improvement of current emerging system is still in its early stages. Firstly, a suitable temperature-responsive material should display switchability when the thermochromic layer reaches the temperature range of ~30 to ~40 °C, accompanied by a drastic and reversible change in optical properties in the NIR range. For materials requiring encapsulation, the encapsulation layer may affect the thermal conduction, resulting the temperature gradient from thermoresponsive materials to the building interior, therefore a more careful design of the transition temperature of the thermal response is needed to maximize the energy-saving capability. Modulation in the visible range is dependent on the specific application circumstances, since it can enhance solar energy modulation ability but the concomitant appearance variation and reduced T_{lum} may or may not be desirable. Moreover, the long-time thermal stability is necessary. Secondly, for the four emerging thermoresponsive reviewed, further research could be explored such as the structure modification to enhance thermochromic properties, which has been much more extensively investigated in VO_2 system. Thirdly, the hybridization between different categories of thermoresponsive materials have been proved successful to further enhance the performance, hence more efforts can be devoted to this direction. Finally, the switch time should be considered for the thermoresponsive material in smart window application. Though there is not a consensus reached, a switch time within several minutes should be acceptable for energy-saving architecture window, considering the relatively slow process of temperature fluctuation in a day. Faster switch property is definitely preferred. Although several materials were reported with the acceptable switch time, such as VO_2, PNIPAm hydrogel, and liquid crystals, the switch time has drawn much less attention than the solar modulation or the

switch temperature. Hence, we encourage to consider the switch time as one of parameters for new thermoresponsive materials in future development.

As for integrated techniques, one direction for further exploration is the combination of active control techniques with thermoresponsive smart windows, which have hitherto been primarily considered as passive devices, controlled by temperature solely. For example, the electro-thermal approach add extra control to cost-effective temperature-responsive smart windows, competing with other commercially available pricey electrochromic devices. However in contrast with one-time switch in electrochromic devices, electro-thermal smart window need constant heating to remain switched which is more energy consuming. How to cut down the energy consumption is a key to promote the electro-thermal windows. Moreover, it is vital by integration performance should not be compromised. The integrated layers may affect transmittance and decrease the solar modulation property. They may also defer the heat transfer, which could affect the switch time as well as the heat retention of windows. Additionally, integrated techniques should address the toxicity and durability issue of the thermochromic layer considering the daily human contact with windows and decades service life of architecture windows. And there are likely to be further, unexplored techniques that could be integrated with thermoresponse to produce more efficient, sustainable, and multifunctional energy-efficient smart windows for buildings as well as other applications. Advances in ease of manufacture and cost-effectiveness for both thermoresponsive and integrated techniques are also necessary to bring these technologies from the laboratory to daily life.

Finally, energy-efficient smart windows hold much promise for contributing to a future, eco-friendly world. However, there is still much work needed to make energy-efficient smart windows a practicable solution. It is hoped that this summary will arouse broader research

interests in this field to accelerate the development of energy-efficient smart windows through application of suitable materials and integrated techniques, by both exploring the tremendous existing library of scientific knowledge and inspiring innovative research for functional devices within and even beyond energy-efficient smart window applications.

Acknowledgements

Y. Ke and C. Zhou contributed equally to this work. This research was supported by Singapore Minster of Education (MOE) Academic Research Fund Tier one, RG124/16 and the National Research Foundation, Prime Minister's Office, Singapore under its Campus for Research Excellence and Technological Enterprise (CREATE) programme.

Received: ((will be filled in by the editorial staff))
Revised: ((will be filled in by the editorial staff))
Published online: ((will be filled in by the editorial staff))

References

[1] a) L. Gao, B. A. Bryan, *Nature* **2017**, *544*, 217; b) A. M. Omer, *Renewable Sustainable Energy Rev.* **2008**, *12*, 2265.

[2] a) L. Pérez-Lombard, J. Ortiz, C. Pout, *Energy Buildings* **2008**, *40*, 394; b) D. M. Kammen, D. A. Sunter, *Science* **2016**, *352*, 922; c) M. Isaac, D. P. van Vuuren, *Energy Policy* **2009**, *37*, 507.

[3] a) Y. Zhai, Y. Ma, S. N. David, D. Zhao, R. Lou, G. Tan, R. Yang, X. Yin, *Science* **2017**, *355*, 1062; b) N. DeForest, A. Shehabi, J. O'Donnell, G. Garcia, J. Greenblatt, E. S. Lee, S. Selkowitz, D. J. Milliron, *Build. Environ.* **2015**, *89*, 107.

[4] a) M. Tarantini, A. D. Loprieno, P. L. Porta, *Energy* **2011**, *36*, 2473; b) R. Baetens, B. P. Jelle, A. Gustavsen, *Sol. Energy Mater. Sol. Cells* **2010**, *94*, 87.

[5] a) B. A. Korgel, *Nature* **2013**, *500*, 278; b) Y. Gao, S. Wang, H. Luo, L. Dai, C. Cao, Y. Liu, Z. Chen, M. Kanehira, *Energy Environ. Sci.* **2012**, *5*, 6104; c) Y. Ke, X. Wen, D. Zhao, R. Che, Q. Xiong, Y. Long, *ACS Nano* **2017**, *11*, 7542; d) N. C. Davy, M. Sezen-Edmonds, J. Gao, X. Lin, A. Liu, N. Yao, A. Kahn, Y.-L. Loo, *Nat. Energy* **2017**, *2*, 17104; e) Q. Liu, Y. Yuan, II. Smalyukh, *Nano Lett.* **2014**, *14*, 4071; f) H. Khandelwal, A. P. H. J. Schenning, M. G. Debije, *Adv. Energy Mater.* **2017**, *7*, 1602209; g) S. Lin, X. Bai, H. Wang, H. Wang, J. Song, K. Huang, C. Wang, N. Wang, B. Li, M. Lei, H. Wu, *Adv. Mater.* **2017**, *29*, 1703238.

[6] a) G. A. Niklasson, C. G. Granqvist, *J. Mater. Chem.* **2007**, *17*, 127; b) S. M. Babulanam, T. S. Eriksson, G. A. Niklasson, C. G. Granqvist, *Sol. Energy Mater.* **1987**, *16*, 347; c) Y. Gao, C. Cao, L. Dai, H. Luo, M. Kanehira, Y. Ding, Z. L. Wang, *Energy Environ. Sci.* **2012**, *5*, 8708; d) H. Kim, Y. Kim, K. S. Kim, H. Y. Jeong, A. R. Jang, S. H. Han, D. H. Yoon, K. S. Suh, H. S. Shin, T. Kim, W. S. Yang, *ACS Nano* **2013**, *7*, 5769.

[7] a) M. Li, S. Magdassi, Y. Gao, Y. Long, *Small* **2017**, *13*, 1701147; b) F. Bella, G. Leftheriotis, G. Griffini, G. Syrrokostas, S. Turri, M. Grätzel, C. Gerbaldi, *Adv. Funct. Mater.* **2016**, *26*, 1127; c) C. J. Barile, D. J. Slotcavage, J. Hou, M. T. Strand, T. S. Hernandez, M. D. McGehee, *Joule* **2017**, *1*, 133; d) C. G. Granqvist, *Thin Solid Films* **2016**, *614*, 90; e) R.-T. Wen, C. G. Granqvist, G. A. Niklasson, *Adv. Funct. Mater.* **2015**, *25*, 3359.

[8] Y. Gao, H. Luo, Z. Zhang, L. Kang, Z. Chen, J. Du, M. Kanehira, C. Cao, *Nano Energy* **2012**, *1*, 221.

[9] a) M. E. A. Warwick, R. Binions, *J. Mater. Chem. A* **2014**, *2*, 3275; b) S. Wang, K. A. Owusu, L. Mai, Y. Ke, Y. Zhou, P. Hu, S. Magdassi, Y. Long, *Appl. Energy* **2018**, *211*, 200.

[10] J. M. Bemmelen, *Zeitschr f Chem und Ind der Kolloide* **1907**, *1*, 213.

[11] a) J. L. Drury, D. J. Mooney, *Biomaterials* **2003**, *24*, 4337; b) W. Yang, H. Yu, G. Li, Y. Wang, L. Liu, *Small* **2017**, *13*, 1602769.

[12] a) M. Hamidi, A. Azadi, P. Rafiei, *Adv. Drug Delivery Rev.* **2008**, *60*, 1638; b) S. Choi, Y. j. Choi, M.-S. Jang, J. H. Lee, J. H. Jeong, J. Kim, *Adv. Funct. Mater.* **2017**, *27*, 1703826.

[13] a) M. W. Tibbitt, K. S. Anseth, *Biotechnol. Bioeng.* **2009**, *103*, 655; b) A. Omidinia-Anarkoli, S. Boesveld, U. Tuvshindorj, J. C. Rose, T. Haraszti, L. De Laporte, *Small* **2017**, *13*, 1702207.

[14] T. S. T. Adams, T. Crook, M. A. M. Cadier, *J. Plast. Reconstr. Aesthet. Surg.* **2007**, *60*, 210.

[15] T.-G. La, X. Li, A. Kumar, Y. Fu, S. Yang, H.-J. Chung, *ACS Appl. Mater. Interfaces* **2017**, *9*, 33100.

[16] a) Y. Zhou, Y. Cai, X. Hu, Y. Long, *J. Mater. Chem. A* **2014**, *2*, 13550; b) Y. Zhou, Y. Cai, X. Hu, Y. Long, *J. Mater. Chem. A* **2015**, *3*, 1121; c) H. Y. Lee, Y. Cai, S. Bi, Y. N. Liang, Y. Song, X. M. Hu, *ACS Appl. Mater. Interfaces* **2017**, *9*, 6054.

[17] Y.-S. Yang, Y. Zhou, F. B. Y. Chiang, Y. Long, *RSC Adv.* **2017**, *7*, 7758.

[18] a) H. G. Schild, D. A. Tirrell, *J. Phys. Chem.* **1990**, *94*, 4352; b) S. S. Pennadam, K. Firman, C. Alexander, D. C. Górecki, *J. Nanobiotechnol.* **2004**, *2*, 8.

[19] a) K. Jain, R. Vedarajan, M. Watanabe, M. Ishikiriyama, N. Matsumi, *Polym. Chem.* **2015**, *6*, 6819; b) C. Wu, S. Zhou, *Macromolecules* **1995**, *28*, 8381; c) X. Wang, C. Wu, *Macromolecules* **1999**, *32*, 4299.

[20] J. Brijitta, B. V. R. Tata, T. Kaliyappan, *J. Nanosci. Nanotechnol.* **2009**, *9*, 5323.

[21] V. R. de la Rosa, P. Woisel, R. Hoogenboom, *Mater. Today* **2015**, *19*, 44.

[22] Y. Zhou, M. Layani, S. Wang, P. Hu, Y. Ke, S. Magdassi, Y. Long, *Adv. Funct. Mater.* **2018**, DOI: 10.1002/adfm.201705365.

[23] Y. Ma, M. Pharr, L. Wang, J. Kim, Y. Liu, Y. Xue, R. Ning, X. Wang, H. U. Chung, X. Feng, J. A. Rogers, Y. Huang, *Small* **2017**, *13*, 1602954.

[24] P. Walden, *Bull. Russ. Acad. Sci.* **1914**, *8*, 1161.

[25] a) R. P. Swatloski, S. K. Spear, J. D. Holbrey, R. D. Rogers, *J. Am. Chem. Soc.* **2002**, *124*, 4974; b) H. Wang, G. Gurau, R. D. Rogers, *Chem. Soc. Rev.* **2012**, *41*, 1519.

[26] X. Sun, H. Luo, S. Dai, *Chem. Rev.* **2012**, *112*, 2100.

[27] a) M. E. V. Valkenburg, R. L. Vaughn, M. Williams, J. S. Wilkes, *Thermochim. Acta* **2005**, *425*, 181; b) P. Wang, S. M. Zakeeruddin, P. Comte, I. Exnar, M. Grätzel, *J. Am. Chem. Soc.* **2003**, *125*, 1166.

[28] a) K. T. Nam, D.-W. Kim, P. J. Yoo, C.-Y. Chiang, N. Meethong, P. T. Hammond, Y.-M. Chiang, A. M. Belcher, *Science* **2006**, *312*, 885; b) M. Armand, F. Endres, D. R. MacFarlane, H. Ohno, B. Scrosati, *Nat. Mater.* **2009**, *8*, 621.

[29] J. Zhu, A. Huang, H. Ma, Y. Ma, K. Tong, S. Ji, S. Bao, X. Cao, P. Jin, *ACS Appl. Mater. Interfaces* **2016**, *8*, 29742.

[30] J. Rocha, Michael W. Anderson, *Eur. J. Inorg. Chem.* **2000**, *5*, 801.

[31] X. Wei, L. Yu, D. Wang, X. Jin, G. Z. Chen, *Green Chem.* **2008**, *10*, 296.

[32] a) J. Zhu, A. Huang, H. Ma, Y. Chen, S. Zhang, S. Ji, S. Bao, P. Jin, *New J. Chem.* **2017**, *41*, 830; b) J. T. Zhu, A. B. Huang, H. B. Ma, S. H. Bao, S. D. Ji, P. Jin, *RSC Adv.* **2016**, *6*, 67396.

[33] T. P. Lodge, *Science* **2008**, *321*, 50.

[34] X. Li, S. Li, Z. Zhang, J. Huang, L. Yang, S.-i. Hirano, *J. Mater. Chem. A* **2016**, *4*, 13822.

[35] H. Y. Lee, Y. Cai, S. Velioglu, C. Mu, C. J. Chang, Y. L. Chen, Y. Song, J. W. Chew, X. M. Hu, *Chem. Mater.* **2017**, *29*, 6947.

[36] a) R. S. Kshetrimayum, *IEEE Potentials* **2005**, *23*, 44; b) T. U. Connell, S. K. Earl, C. Ng, A. Roberts, T. J. Davis, J. M. White, A. Polyzos, D. E. Gómez, *Small* **2017**, *13*, 1700692.

[37] a) M. A. Antoniades, G. V. Eleftheriades, *IEEE Antennas Wireless Propag. Lett.* **2008**, *7*, 425; b) H. F. Ma, X. Chen, H. S. Xu, X. M. Yang, W. X. Jiang, T. J. Cui, *Appl. Phys. Lett.* **2009**, *95*, 094107.

[38] a) J. Hao, J. Wang, X. Liu, W. J. Padilla, L. Zhou, M. Qiu, *Appl. Phys. Lett.* **2010**, *96*, 251104; b) N. I. Landy, S. Sajuyigbe, J. J. Mock, D. R. Smith, W. J. Padilla, *Phys. Rev. Lett.* **2008**, *100*, 207402.

[39] a) H. Chen, C. T. Chan, *Appl. Phys. Lett.* **2007**, *91*, 183518; b) D. Schurig, J. J. Mock, B. J. Justice, S. A. Cummer, J. B. Pendry, A. F. Starr, D. R. Smith, *Science* **2006**, *314*, 977.

[40] X. Liu, W. J. Padilla, *Adv. Mater.* **2016**, *28*, 871.

[41] a) J. L. Silverberg, A. A. Evans, L. McLeod, R. C. Hayward, T. Hull, C. D. Santangelo, I. Cohen, *Science* **2014**, *345*, 647; b) C. Lv, D. Krishnaraju, G. Konjevod, H. Yu, H. Jiang, *Sci.*

Rep. **2014**, *4*, 5979; c) J. T. B. Overvelde, T. A. de Jong, Y. Shevchenko, S. A. Becerra, G. M. Whitesides, J. C. Weaver, C. Hoberman, K. Bertoldi, *Nat. Commun.* **2016**, *7*, 10929.

[42] Y. Tang, G. Lin, S. Yang, Y. K. Yi, R. D. Kamien, J. Yin, *Adv. Mater.* **2017**, *29*, 1604262.

[43] a) A. S. Bhalla, R. Guo, R. Roy, *Mater. Res. Innovations* **2000**, *4*, 3; b) X. Zhang, L. B. Abdalla, Q. Liu, A. Zunger, *Adv. Funct. Mater.* **2017**, *27*, 1701266; c) W. Tian, H. Zhou, L. Li, *Small* **2017**, *13*, 1702107.

[44] a) W. Wang, D. Zhao, F. Zhang, L. Li, M. Du, C. Wang, Y. Yu, Q. Huang, M. Zhang, L. Li, J. Miao, Z. Lou, G. Shen, Y. Fang, Y. Yan, *Adv. Funct. Mater.* **2017**, *27*, 1703953; b) Q. Luo, H. Ma, F. Hao, Q. Hou, J. Ren, L. Wu, Z. Yao, Y. Zhou, N. Wang, K. Jiang, H. Lin, Z. Guo, *Adv. Funct. Mater.* **2017**, *27*, 1703068.

[45] P. J. Dereń, A. Bednarkiewicz, P. Goldner, O. Guillot-Noël, *J. Appl. Phys.* **2008**, *103*, 043102.

[46] a) S. D. Stranks, H. J. Snaith, *Nat. Nanotechnol.* **2015**, *10*, 391; b) M. Yuan, L. N. Quan, R. Comin, G. Walters, R. Sabatini, O. Voznyy, S. Hoogland, Y. Zhao, E. M. Beauregard, P. Kanjanaboos, Z. Lu, D. H. Kim, E. H. Sargent, *Nat. Nanotechnol.* **2016**, *11*, 872.

[47] a) J. Luo, J.-H. Im, M. T. Mayer, M. Schreier, M. K. Nazeeruddin, N.-G. Park, S. D. Tilley, H. J. Fan, M. Grätzel, *Science* **2014**, *345*, 1593; b) G. Tsekouras, D. Neagu, J. T. S. Irvine, *Energy Environ. Sci.* **2013**, *6*, 256.

[48] N. Ahn, S. M. Kang, J.-W. Lee, M. Choi, N.-G. Park, *J. Mater. Chem. A* **2015**, *3*, 19901.

[49] M. De Bastiani, M. I. Saidaminov, I. Dursun, L. Sinatra, W. Peng, U. Buttner, O. F. Mohammed, O. M. Bakr, *Chem. Mater.* **2017**, *29*, 3367.

[50] a) G. E. Eperon, V. M. Burlakov, A. Goriely, H. J. Snaith, *ACS Nano* **2014**, *8*, 591; b) X. Hu, X. Zhang, L. Liang, J. Bao, S. Li, W. Yang, Y. Xie, *Adv. Funct. Mater.* **2014**, *24*, 7373.

[51] G. Maculan, A. D. Sheikh, A. L. Abdelhady, M. I. Saidaminov, M. A. Haque, B. Murali, E. Alarousu, O. F. Mohammed, T. Wu, O. M. Bakr, *J. Phys. Chem. Lett.* **2015**, *6*, 3781.

[52] A. Halder, D. Choudhury, S. Ghosh, A. S. Subbiah, S. K. Sarkar, *J. Phys. Chem. Lett.* **2015**, *6*, 3180.

[53] J. Lin, M. Lai, L. Dou, C. S. Kley, H. Chen, F. Peng, J. Sun, D. Lu, S. A. Hawks, C. Xie, F. Cui, A. P. Alivisatos, D. T. Limmer, P. Yang, *Nat. Mater.* **2018**, *17*, 261.

[54] K. Binnemans, *Chem. Rev.* **2005**, *105*, 4148.

[55] M. J. Stephen, J. P. Straley, *Rev. Mod. Phys.* **1974**, *46*, 617.

[56] a) J. Yan, F. Ota, B. A. San Jose, K. Akagi, *Adv. Funct. Mater.* **2017**, *27*, 1604529; b) Q. Liu, I. I. Smalyukh, *Sci. Adv.* **2017**, *3*, e1700981; c) H. Liu, Y. Tang, C. Wang, Z. Xu, C. Yang, T. Huang, F. Zhang, D. Wu, X. Feng, *Adv. Funct. Mater.* **2017**, *27*, 1606269.

[57] H. Khandelwal, A. P. H. J. Schenning, M. G. Debije, *Adv. Energy Mater.* **2017**, *7*, 1602209.

[58] H. Kakiuchida, M. Tazawa, K. Yoshimura, A. Ogiwara, *Sol. Energy Mater. Sol. Cells* **2010**, *94*, 1747.

[59] J. Sun, H. Wang, L. Wang, H. Cao, H. Xie, X. Luo, J. Xiao, H. Ding, Z. Yang, H. Yang, *Smart Mater. Struct.* **2014**, *23*, 125038.

[60] S. Guo, X. Liang, C. Zhang, M. Chen, C. Shen, L. Zhang, X. Yuan, B. He, H. Yang, *ACS Appl. Mater. Interfaces* **2017**, *9*, 2942.

[61] X. Liang, S. Guo, M. Chen, C. Li, Q. Wang, C. Zou, C. Zhang, L. Zhang, S. Guo, H. Yang, *Mater. Horiz.* **2017**, *4*, 878.

[62] X. Liang, C. Guo, M. Chen, S. Guo, L. Zhang, F. Li, S. Guo, H. Yang, *Nanoscale Horiz.* **2017**, *2*, 319.

[63] X. Liang, M. Chen, S. Guo, L. Zhang, F. Li, H. Yang, *ACS Appl. Mater. Interfaces* **2017**, *9*, 40810.

[64] a) N. B. Aetukuri, A. X. Gray, M. Drouard, M. Cossale, L. Gao, A. H. Reid, R. Kukreja, H. Ohldag, C. A. Jenkins, E. Arenholz, K. P. Roche, H. A. Dürr, M. G. Samant, S. S. P. Parkin, *Nat. Phys.* **2013**, *9*, 661; b) J. H. Park, J. M. Coy, T. S. Kasirga, C. Huang, Z. Fei, S. Hunter, D. H. Cobden, *Nature* **2013**, *500*, 431.

[65] C. Liu, Y. Long, S. Magdassi, D. Mandler, *Nanoscale* **2017**, *9*, 485.

[66] Y. Ke, I. Balin, N. Wang, Q. Lu, A. I. Tok, T. J. White, S. Magdassi, I. Abdulhalim, Y. Long, *ACS Appl. Mater. Interfaces* **2016**, *8*, 33112.

[67] a) G. Cai, J. Wang, P. S. Lee, *Acc. Chem. Res.* **2016**, *49*, 1469; b) G. Cai, P. Darmawan, X. Cheng, P. S. Lee, *Adv. Energy Mater.* **2017**, *7*, 1602598.

[68] a) L. Kang, Y. Gao, H. Luo, Z. Chen, J. Du, Z. Zhang, *ACS Appl. Mater. Interfaces* **2011**, *3*, 135; b) X. Cao, N. Wang, J. Y. Law, S. C. J. Loo, S. Magdassi, Y. Long, *Langmuir* **2014**, *30*, 1710.

[69] a) C. Liu, X. Cao, A. Kamyshny, J. Y. Law, S. Magdassi, Y. Long, *J. Colloid Interface Sci.* **2014**, *427*, 49; b) S. Y. Li, G. A. Niklasson, C. G. Granqvist, *J. Appl. Phys.* **2011**, *109*, 113515; c) Y. Gao, S. Wang, L. Kang, Z. Chen, J. Du, X. Liu, H. Luo, M. Kanehira, *Energy Environ. Sci.* **2012**, *5*, 8234; d) Z. Chen, Y. Gao, L. Kang, C. Cao, S. Chen, H. Luo, *J. Mater. Chem. A* **2014**, *2*, 2718.

[70] a) A. Taylor, I. Parkin, N. Noor, C. Tummeltshammer, M. S. Brown, I. Papakonstantinou, *Opt. Express* **2013**, *21*, A750; b) X. Qian, N. Wang, Y. Li, J. Zhang, Z. Xu, Y. Long, *Langmuir* **2014**, *30*, 10766.

[71] a) N. R. Mlyuka, G. A. Niklasson, C. G. Granqvist, *Appl. Phys. Lett.* **2009**, *95*, 171909; b) N. Wang, M. Duchamp, R. E. Dunin-Borkowski, S. Liu, X. Zeng, X. Cao, Y. Long, *Langmuir* **2016**, *32*, 759; c) X. Cao, N. Wang, S. Magdassi, D. Mandler, Y. Long, *Sci. Adv. Mater.* **2014**, *6*, 558.

[72] C. Liu, I. Balin, S. Magdassi, I. Abdulhalim, Y. Long, *Opt. Express* **2015**, *23*, A124.

[73] a) X. Wang, Y. Ke, H. Pan, K. Ma, Q. Xiao, D. Yin, G. Wu, M. T. Swihart, *ACS Catal.* **2015**, *5*, 2534; b) X. Wang, X. Liu, D. Yin, Y. Ke, M. T. Swihart, *Chem. Mater.* **2015**, *27*, 3378.

[74] a) N. Wang, S. Liu, X. T. Zeng, S. Magdassi, Y. Long, *J. Mater. Chem. C* **2015**, *3*, 6771; b) N. Wang, M. Duchamp, C. Xue, R. E. Dunin Borkowski, G. Liu, Y. Long, *Adv. Mater. Interfaces* **2016**, *3*, 1600164.

[75] C. Wu, F. Feng, Y. Xie, *Chem. Soc. Rev.* **2013**, *42*, 5157.

[76] J. D. Budai, J. Hong, M. E. Manley, E. D. Specht, C. W. Li, J. Z. Tischler, D. L. Abernathy, A. H. Said, B. M. Leu, L. A. Boatner, R. J. McQueeney, O. Delaire, *Nature* **2014**, *515*, 535.

[77] Y. Zhou, M. Layani, F. Y. C. Boey, I. Sokolov, S. Magdassi, Y. Long, *Adv. Mater. Technol.* **2016**, *1*, 1600069.

[78] S. Zheng, D. Wang, Y. Tian, L. Jiang, *Adv. Funct. Mater.* **2016**, *26*, 9018.

[79] a) Z. Chen, C. Cao, S. Chen, H. Luo, Y. Gao, *J. Mater. Chem. A* **2014**, *2*, 11874; b) Y. Li, S. Ji, Y. Gao, H. Luo, M. Kanehira, *Sci. Rep.* **2013**, *3*, 1370; c) X. Lu, Y. Sun, Z. Chen, Y. Gao, *Sol. Energy Mater. Sol. Cells* **2017**, *159*, 102; d) Z. Zhang, Y. Gao, H. Luo, L. Kang, Z. Chen, J. Du, M. Kanehira, Y. Zhang, Z. L. Wang, *Energy Environ. Sci.* **2011**, *4*, 4290.

[80] M. J. Powell, R. Quesada-Cabrera, A. Taylor, D. Teixeira, I. Papakonstantinou, R. G. Palgrave, G. Sankar, I. P. Parkin, *Chem. Mater.* **2016**, *28*, 1369.

[81] Y. Chen, X. Zeng, J. Zhu, R. Li, H. Yao, X. Cao, S. Ji, P. Jin, *ACS Appl. Mater. Interfaces* **2017**, *9*, 27784.

[82] J. Zheng, S. Bao, P. Jin, *Nano Energy* **2015**, *11*, 136.

[83] a) H. Zhou, J. Li, S. Bao, J. Li, X. Liu, P. Jin, *Appl. Surf. Sci.* **2016**, *363*, 532; b) L. Kang, Y. Gao, H. Luo, J. Wang, B. Zhu, Z. Zhang, J. Du, M. Kanehira, Y. Zhang, *Sol. Energy Mater. Sol. Cells* **2011**, *95*, 3189.

[84] C. Liu, N. Wang, Y. Long, *Appl. Surf. Sci.* **2013**, *283*, 222.

[85] M. Liu, S. Wang, L. Jiang, *Nat. Rev. Mater.* **2017**, *2*, 17036.

[86] a) S.-Y. Wu, S.-K. Su, C.-J. Chang, C.-H. Huang, J.-K. Chen, *Ceram. Int.* **2016**, *42*, 17610; b) Z. Liang, L. Zhao, W. Meng, C. Zhong, S. Wei, B. Dong, Z. Xu, L. Wan, S. Wang, *J. Alloys Compd.* **2017**, *694*, 124; c) Y. Lu, X. Xiao, Y. Zhan, Z. Gao, H. Cheng, C. Huan, S. Qi, G. Xu, *Ceram. Int.* **2018**, *44*, 1013.

[87] a) J. Zhou, Y. Gao, Z. Zhang, H. Luo, C. Cao, Z. Chen, L. Dai, X. Liu, *Sci. Rep.* **2013**, *3*, 3029; b) F. Guo, S. Chen, Z. Chen, H. Luo, Y. Gao, T. Przybilla, E. Spiecker, A. Osvet, K. Forberich, C. J. Brabec, *Adv. Opt. Mater.* **2015**, *3*, 1524.

[88] M. Li, H. Wu, L. Zhong, H. Wang, Y. Luo, G. Li, *J. Mater. Chem. C* **2016**, *4*, 1579.

[89] M. Li, S. Ji, J. Pan, H. Wu, L. Zhong, Q. Wang, F. Li, G. Li, *J. Mater. Chem. A* **2014**, *2*, 20470.

[90] Y. Chen, L. Fan, Q. Fang, W. Xu, S. Chen, G. Zan, H. Ren, L. Song, C. Zou, *Nano Energy* **2017**, *31*, 144.

[91] S. Kiruthika, G. U. Kulkarni, *Sol. Energy Mater. Sol. Cells* **2017**, *163*, 231.

[92] A. K. Singh, S. Kiruthika, I. Mondal, G. U. Kulkarni, *J. Mater. Chem. C* **2017**, *5*, 5917.

[93] a) A. Seeboth, D. Lotzsch, R. Ruhmann, O. Muehling, *Chem. Rev.* **2014**, *114*, 3037; b) K. Ueno, K. Matsubara, M. Watanabe, Y. Takeoka, *Adv. Mater.* **2007**, *19*, 2807; c) M. Mitov,

Adv. Mater. **2012**, *24*, 6260; d) X. Luo, J. Li, C. Li, L. Heng, Y. Q. Dong, Z. Liu, Z. Bo, B. Z. Tang, *Adv. Mater.* **2011**, *23*, 3261; e) G. Zhang, J. M. W. Chan, *J. Mater. Chem. C* **2017**, *5*, 10007; f) U. Jonas, K. Shah, S. Norvez, D. H. Charych, *J. Am. Chem. Soc.* **1999**, *121*, 4580; g) S. Okada, S. Peng, W. Spevak, D. Charych, *Acc. Chem. Res.* **1998**, *31*, 229.

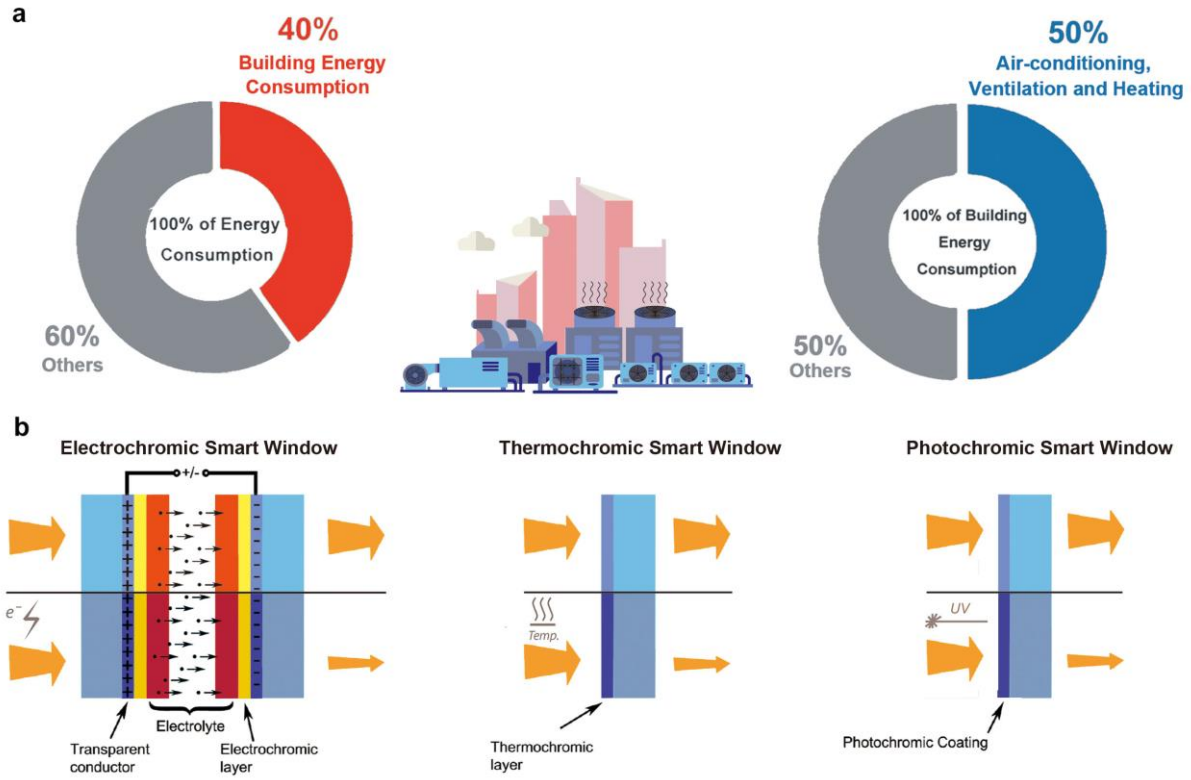

Figure 1. a) Proportion of building energy consumption compared with total energy consumption. Proportion of energy consumption of building services such as heating, ventilation, and air conditioning of total building energy consumption. b) Schematic of electrochromic, thermochromic and photochromic smart windows. The orange arrows indicate incident sunlight. Reproduced with permission.[7a] Copyright 2017, John Wiley & Sons.

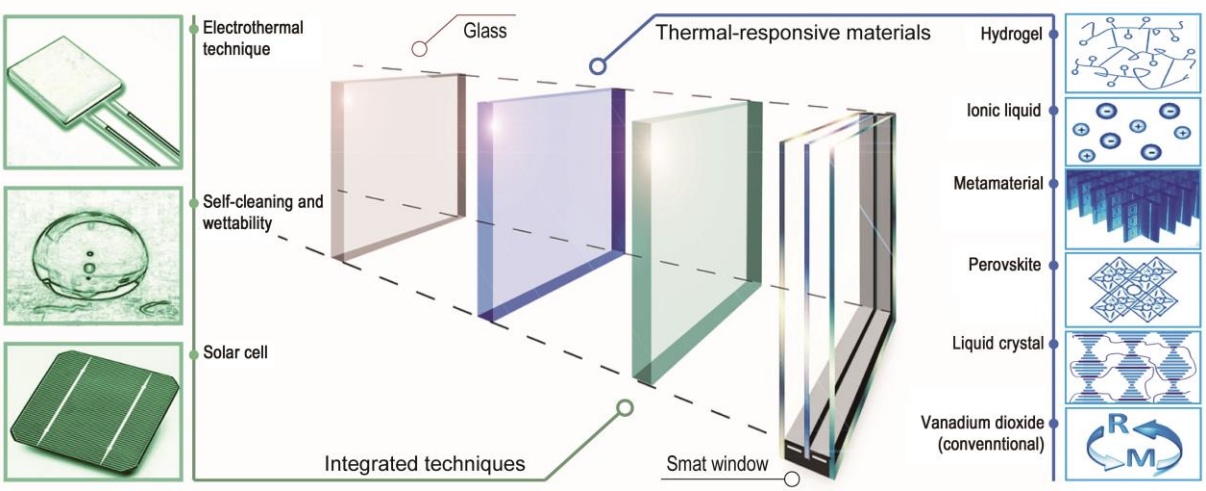

Figure 2. Schematic outline of the two key components of energy-efficient smart windows: thermoresponsive materials and integrated techniques. Emerging materials include hydrogels, ionic liquids, metamaterials, perovskites, and liquid crystals. The conventional VO_2 is briefly discussed as a reference.

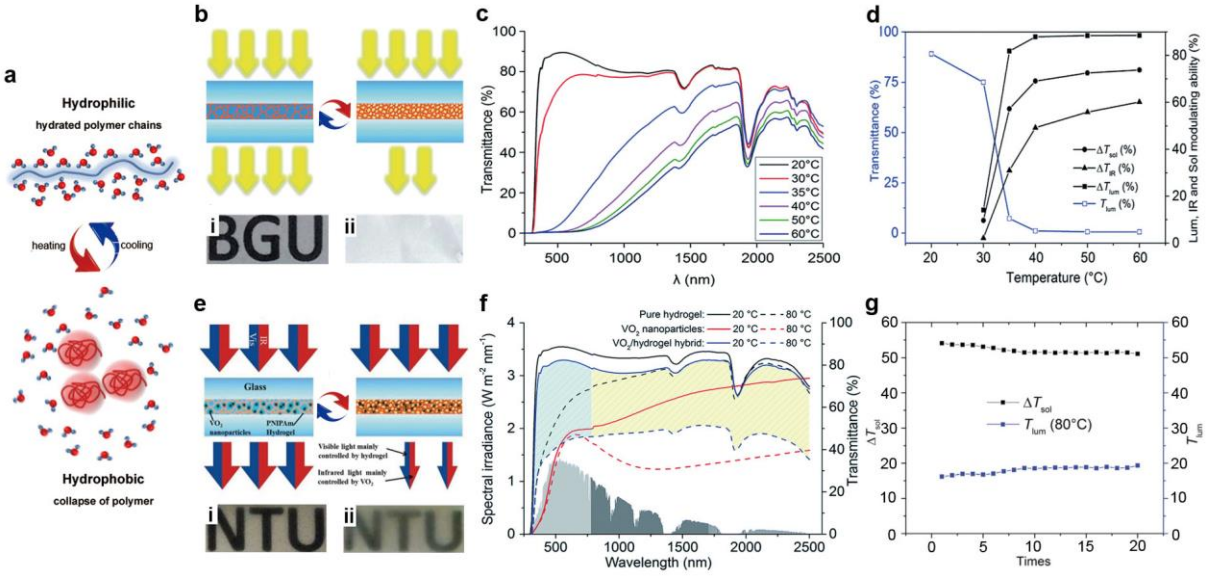

Figure 3. a) Schematic of the responsive polymer chain behavior below and above the LSCT. The top image shows the polymer chains at relatively low temperature surrounded by water molecules, and the bottom image shows the loss of water molecules and collapse of polymer chains to form polymer clusters when the temperature is elevated above the LSCT. Reproduced with permission.[21] Copyright 2016, Elsevier. b) Schematic diagram of the PNIPAm hydrogel smart window sandwich structure. The glass substrates are represented in blue and the hydrogel (red network) aggregates at elevated temperature. Incident light (golden arrows) passes through the hydrogel below 32 °C, but is largely blocked above 32 °C. The insets i and ii are the 200 μm demonstration devices at 20 and 80 °C, respectively. c) Transmittance spectrum of 200 μm PNIPAm hydrogel thin film at temperatures varying from 20 to 60 °C. d) Optical properties of integrated visible transmittance (T_{lum}), calculated solar energy modulation (ΔT_{sol}), infrared modulation (ΔT_{IR}), and integrated visible light modulation (ΔT_{lum}) of 200 μm PNIPAm film at temperatures ranging from 20 to 60 °C. Figure 3d is calculated based on the measured transmittance spectra in 3c. Reproduced with

permission.[16a] Copyright 2014, Royal Society of Chemistry. e) Schematic diagram of the PNIPAm-VO_2 hybrid hydrogel smart window sandwich structure. The insets i and ii demonstrate PNIPAm-VO_2 hybrid thin films at room temperature and 35°C respectively. f) UV-Vis-NIR transmittance spectra of pure PNIPAm hydrogel, VO_2 nanoparticles and VO_2-PNIPAm hybrid hydrogel at 20 and 80 °C. g) Durability test of 100 μm PNIPAm-VO_2 hybrid film with temperature variation between 20 and 80 °C. Reproduced with permission.[16b] Copyright 2015, Royal Society of Chemistry.

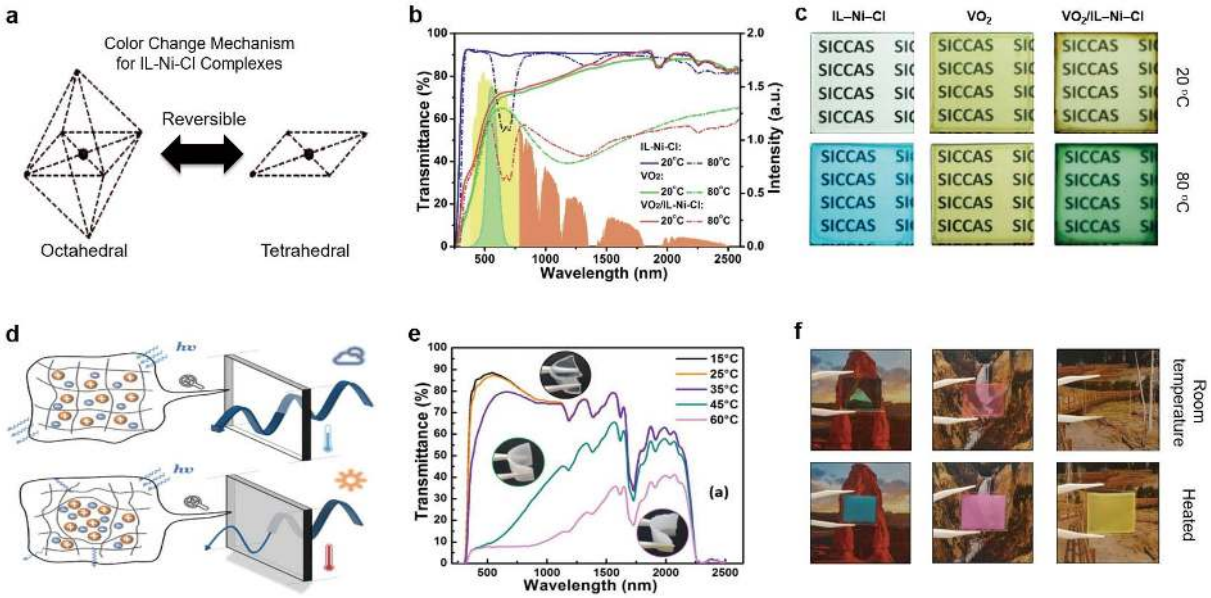

Figure 4. (a) Schematic illustration of octahedral-tetrahedral configuration change of ionic liquid-based complex system. The IL-Ni-Cl complex undergoes a phase transition from octahedral to tetrahedral above the LCST. (b) Transmittance spectrum over the UV-Vis-NIR regions of pure IL-Ni-Cl film, VO_2 nanoparticles and VO_2/IL-Ni-Cl hybrid film at 20 and 80 °C. (c) Demonstrations of pure IL-Ni-Cl film, VO_2 nanoparticle film and VO_2/IL-Ni-Cl hybrid film at 20 and 80 °C. Reproduced with permission.[29] Copyright 2016, American Chemical Society. (d) Schematic illustration of thermochromic optical transmittance change upon variation in temperature. Decreased transparency of the ionogel above the LCST results from light scattering at interfaces of ionic liquid and polymer chains. (e) Transmittance spectrum over the UV-Vis-NIR region of ionogel at various temperatures ranging from 15-60 °C. The insets are the photographs of transparent, translucent and opaque states of the ionogel, respectively. (f) Demonstration of ionogel films mixed with brilliant green, rhodamine B (RhB) and methyl orange organic dyes below and above the transition temperature, respectively. Reproduced with permission.[35] Copyright 2017, American Chemical Society.

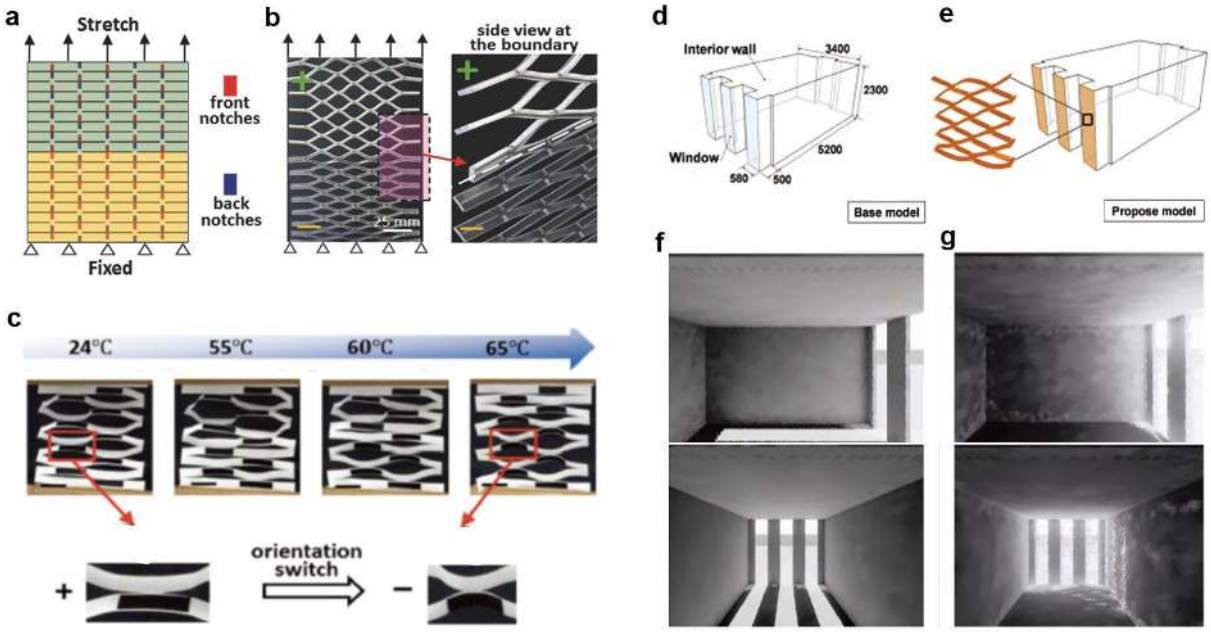

Figure 5. a) Schematic illustration of kiri-kirigami structure with notches on both sides. The upper part (green) has reversed patterned notches compared with the lower part (yellow). b) Optical images of the deformed kiri-kirigami structure with identical design to (a) upon uniaxial stretching. c) Experimental demonstrations of thermal activation and orientation switch of kiri-kirigami paper metamaterials at various temperatures. d-g) Simulation of building energy consumption while kiri-kirigami metamaterials are applied as the thermoresponsive building envelope. Schematic illustration of the stimulation space, (d) without (base model) and (e) with kiri-kirigami (proposed model) smart windows. Performance in the stimulation space of the (f) base model and (g) proposed model at noon. Reproduced with permission.[42] Copyright 2016, John Wiley & Sons.

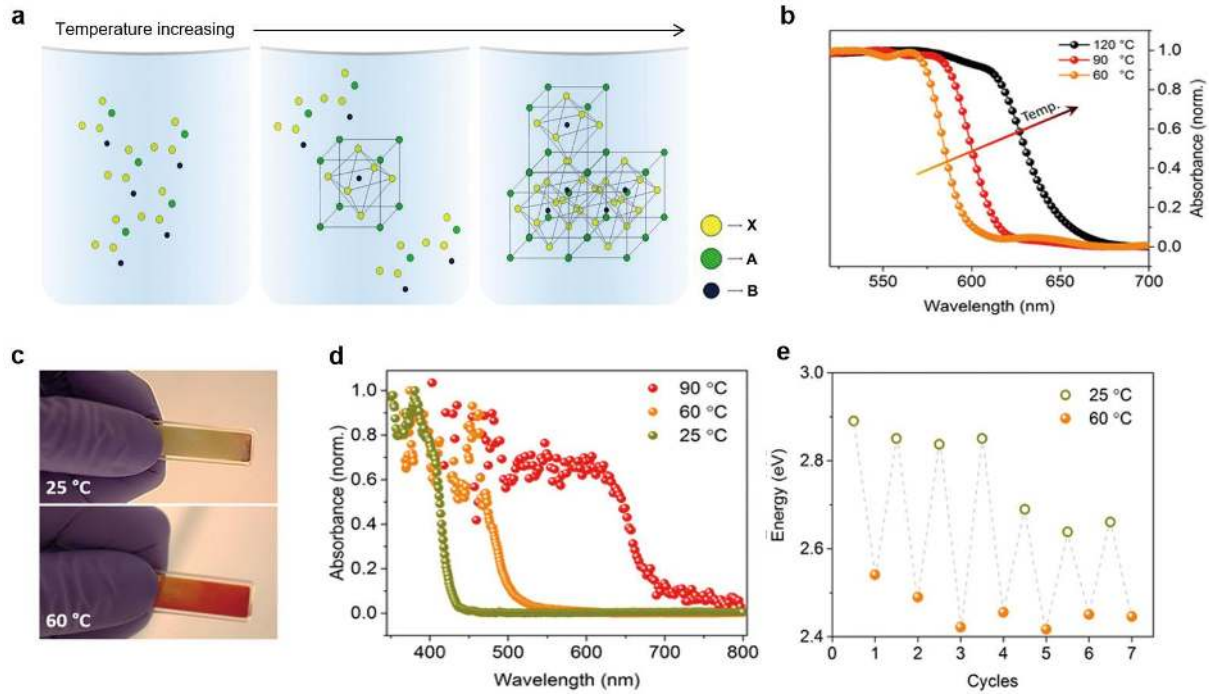

Figure 6. a) Schematic illustration of the inverse temperature crystallization (ITC) process of perovskite materials: with increasing temperature, the perovskite crystals nucleate and grow. b) Absorption spectra of perovskite crystals obtained from inks at 60, 90 and 120 °C. c) Photographs of thermochromic prototype annealed at 25 °C (top) and 60 °C (bottom). d) Absorption spectra of the thermochromic prototype after annealing at the indicated temperature. e) Band edge alternation of the thermochromic prototype during heating and cooling cycles between 25 and 60 °C. The green circles represent the extrapolated maxima at 25 °C; the red spots represent the extrapolated minima at 60 °C. Reproduced with permission.[49] Copyright 2017, American Chemical Society.

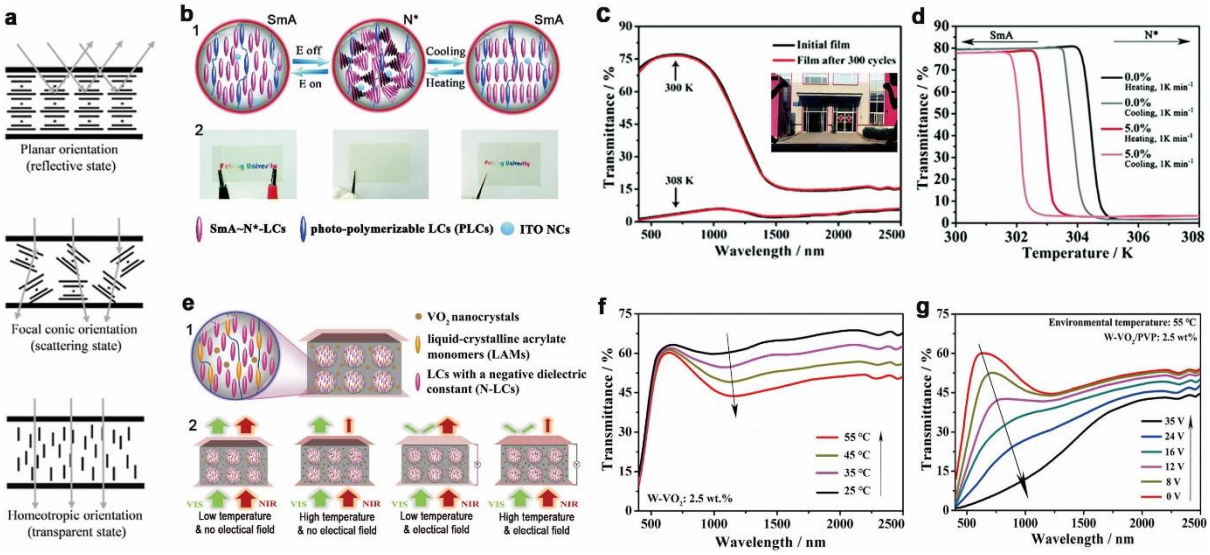

Figure 7. a) Schematic of the orientation-dependent optical behavior of cholesteric liquid crystalline materials. Reproduced with permission. [57] Copyright 2017, John Wiley & Sons. b) Schematic of the smectic A (SmA) to chiral nematic (N*) phase transition in a cell containing the liquid crystals (LCs) and indium tin oxide (ITO) nanocrystals (NCs). The transition can be reversibly induced by either electric- or thermal-stimulus (b1), accompanying with distinct transparency change, demonstrated as the corresponding photographs (b2). c) Temperature-dependent transmittance spectra of the smart film consisting 5 wt% ITO NCs before and after 300 cycles. Inset of (c) is the photography of the meter-scale film. d) Temperature-resolved transmittance at 560 nm of smart films containing 0% and 5 wt% ITO NCs. Reproduced with permission. [61] Copyright 2017, Royal Society of Chemistry. e) Schematic of the VO_2-LCs composite film (e1) with four optical states under different stimuli (e2). f) Temperature-dependent spectra of the composite film containing 2.5wt% W-doped VO_2. g) Electric-field-dependent of the transmittance spectra of the composite film containing 2.5wt% W-doped VO_2 at 55 ºC. Reproduced with permission. [63] Copyright 2017, Royal Society of Chemistry.

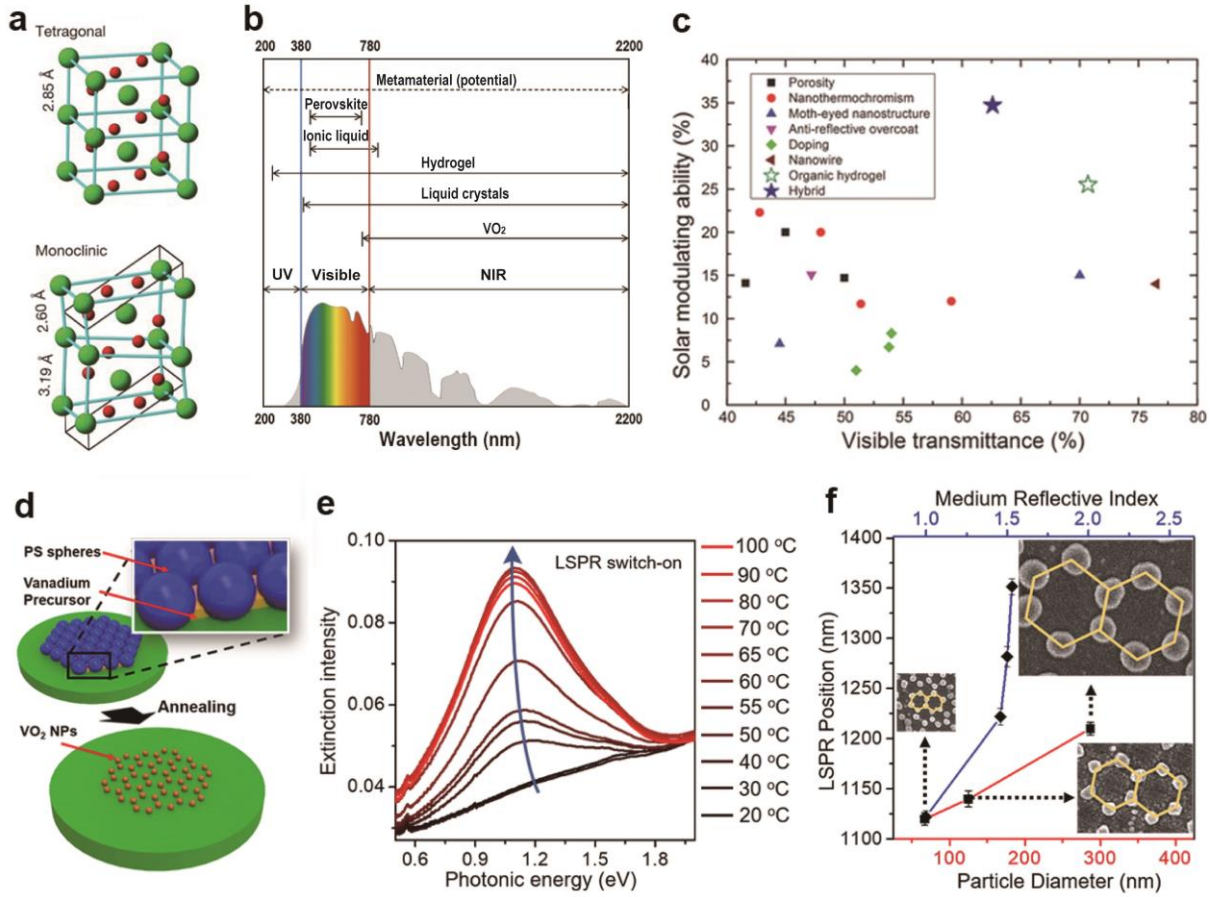

Figure 8. a) Crystal structures of tetragonal (top) and monoclinic (bottom) VO_2. b) Summary of the spectral ranges that can be modulated by metamaterials, perovskites, ionic liquids, hydrogels, liquid crystals, and VO_2. Reproduced with permission.[76] Copyright 2014, Nature Publishing Group. For the metamaterials, the potential spectral range is indicated since accurate data is not available. c) Summary of quality data on solar energy modulation ability (ΔT_{sol}) and visible transmittance reported for methods including porosity, nanotherchromism, moth-eye nanostructure, anti-reflective overcoat, doping, nanowire, organic hydrogel, and VO_2/hydrogel hybrid. Reproduced with permission.[77] Copyright 2016, John Wiley & Sons. d) Illustration of the preparation method of VO_2 nanoparticles (NPs) through the sacrificial two-dimensional colloidal templates made by polystyrene (PS) spheres. e) The temperature-dependent extinction of hexagonal patterned VO_2 NPs with an average diameter of 67 nm. The localized surface plasmon resonance (LSPR) rises upon increasing temperature. f) The LSPR position of hexagonal patterned VO_2 NPs in relation to particle diameter and medium reflective index. Insets are scanning electron microscopy (SEM) images of patterned VO_2 NPs with average diameters of 67, 125, and 287 nm. Reproduced with permission.[5c] Copyright 2017, American Chemical Society.

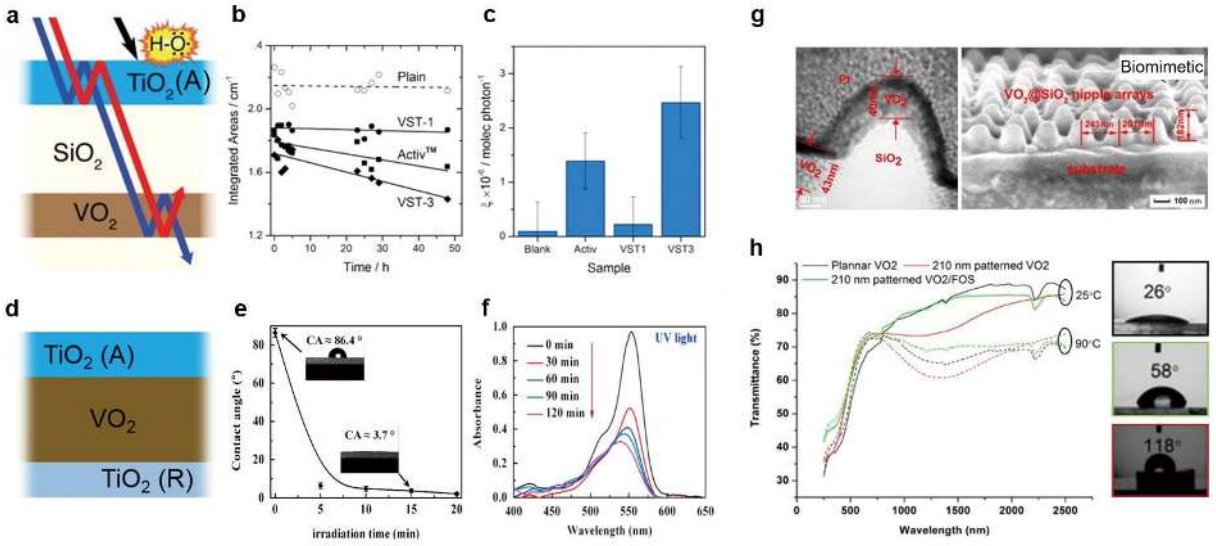

Figure 9. a) Illustration of the $VO_2/SiO_2/TiO_2$(A) multilayer for self-cleaning and energy-saving coatings. b) and c) Degradation of stearic acid under UV illumination (I=4 mW cm^{-2}) on $VO_2/SiO_2/TiO_2$(R) (VST-1), $VO_2/SiO_2/TiO_2$(A) (VST-3), plain (blank), and Pilkington Activ glass (Activ): b) Time-dependent integrated area of stearic acid; c) The calculated corresponding formal quantum efficiency (ξ), presenting the molecular quantity of degraded stearic acid per incident photon. Reproduced with permission.[80] Copyright 2014, American Chemical Society. d) Illustration of the TiO_2(A)/VO_2/TiO_2(R) multilayer. e) Time-resolved contact angle change on the TiO_2(A) surface with hydrocarbon adsorbates. f) Absorbance spectra of rhodamine B (RhB) on the TiO_2(A) surface under a constant UV light irradiation with increasing time. Reproduced with permission.[82] Copyright 2015, Elsevier. g) TEM image of an individual VO_2-coated SiO_2 nipple nanostructure (left) and SEM image of the nipple array with 210 nm periodicity (right). h) Transmittance spectra at 25 and 90 °C (left) as well as contact angle measurements (right) of planar VO_2, 210 nm-patterned VO_2 and 210 nm-patterned VO_2/FOS. Reproduce with permission.[70b] Copyright 2014, American Chemical Society.

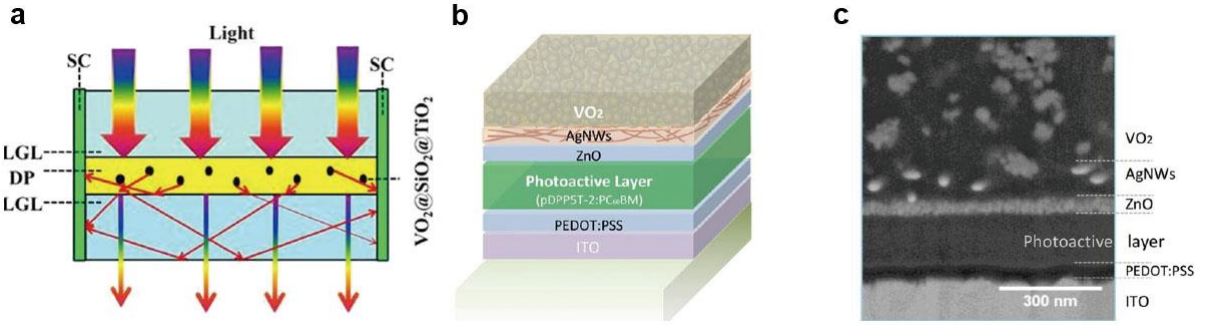

Figure 10. a) Illustration of the integrated SC and VO_2-based thermochromic film utilizing light scattering. The light guide layer (LGL) and the low reflective index medium (DP) are made of polycarbonate (PC) and VO_2/polyurethane (PU) composite, respectively. Some of the incident light is scattered to the SCs. Reproduced with permission.[87a] Copyright 2013, Nature Publishing Group. b) Illustration of the layered integration of SC and VO_2-based thermochromic films utilizing light transmittance. pDPP5T-2:PC_{60}BM and PEDOT:PSS refer to the diketopyrrolopyrrole-quinquethiophene alternating copolymer:[6,6]-phenyl-C_{60}-butyric acid methyl ester and poly(3,4-ethylenedioxythiophene):polystyrene sulfonate, respectively.

c) The cross sectional SEM image of the multilayer configuration corresponding to the illustration of (b). Reproduced with permission. Copyright 2015,[87b] John Wiley & Sons.

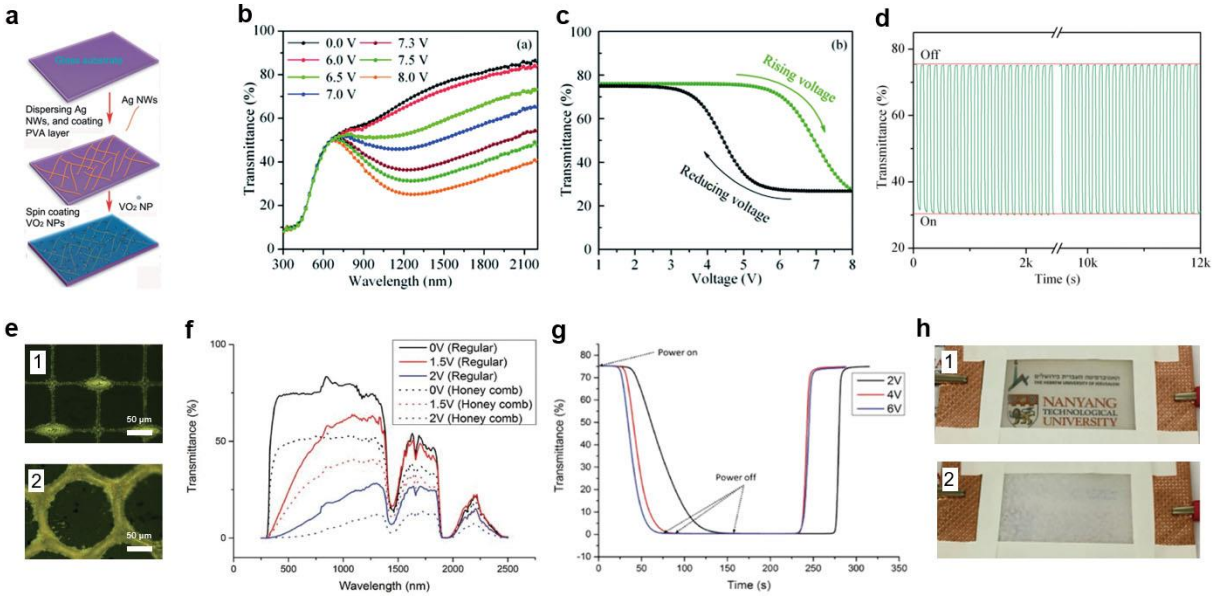

Figure 11. a) Schematic representation of a VO_2/Ag-based electro-thermochromic device and its fabrication process. Firstly, Ag nanowires are deposited on the pre-cleaned glass substrate, followed by a thin layer of polyvinyl alcohol (PVA). The VO_2 nanoparticles are deposited on top of the PVA film by spin coating. b) UV-Vis-NIR transmittance spectrum of the VO_2/Ag based electro-thermochromic device at various voltages from 0 to 8 V. c) Transmittance hysteresis loop of the VO_2/Ag-based electro-thermochromic device as a function of applied voltage at a wavelength of 1.5 μm. d) Infrared response of the VO_2/Ag based electro-thermochromic device with 8 V applied voltage at 1.5 μm. Reproduced with permission.[89] Copyright 2014, Royal Society of Chemistry. e) Optical microscope images of self-assembled electrodes in (1) square and (2) honeycomb shapes. f) Transmittance spectra of hydrogel-based electro-thermochromic devices with different electrode alignments at 0-2 V applied voltage. g) Response time of square shaped hydrogel-based electro-thermochromic device with 2-6 V applied voltage. h) Demonstration of hydrogel-based electro-thermochromic device (1) with and (2) without voltage applied. Reproduced with permission.[77] Copyright 2016, John Wiley & Sons.

Authors:

 Yujie Ke obtained his Bachelor and Master degrees from Wuhan Institute of Technology, China in 2013 and University at Buffalo, the State University of New York (SUNY-Buffalo), US in 2015, respectively. Currently, he is a Ph.D. candidate in Nanyang Technological University (NTU), Singapore under the guidance of Dr. Yi Long. His research interest includes smart windows, thermochromism, and stimulus-responsive materrials.

 Dr. Siew Hwa Chan is now a Full Professor in the Schooll of Mechanical and Aerospace Engineering at NTU. He is concurrently holding 2 appointments as the Co-Director of the Energy Research Institute at NTU (ERI@N), and the Deputy Director of Martime Institute at NTU (MI@NTU). He jonied NTU in 1991 after obtaining his Ph.D. and subsequently working as a postdoctoral researher at Imperial College London, UK. His research is focused on applied thermo-science and electrochemical convension, in particular the fuel cells and electrolyzers.

 Dr. Yi Long is a Senior Lecturer in the School of Materials Science and Engineering at NTU. She obtained her Ph.D. degree from the University of Cambridge, UK. Her research focuses on nanos- tructured functional materials and thin films. She has successfully implemented technology transfer from lab to industry for hard-disk Company and car grooming Company. Her recent research is to develop energy-saving coatings, including VO_2 thin films.

The table of contents entry:

Smart windows are promised significant contribution to the economization of building energy consumption. The rapid development of thermoresonsive materials and integrated techniques provide novel directions beyond conventional pure VO_2-based thermochromic smart windows. The review summarizes emerging materials, including hydrogels, ionic liquids, perovskites, and metamaterials and integrated techniques, covering electro-thermal devices, self-cleaning, wettability, and integration with solar cells.

Keyword

smart window, thermochromism, perovskite, metamaterial, hydrogel

Author

*Yujie Ke,[1,] Chengzhi Zhou,[2,3] Yang Zhou,[1] Shancheng Wang,[1] Siew Hwa Chan,[3] Yi Long.[1,4,] **

[1] School of Materials Science and Engineering, Nanyang Technological University, 50 Nanyang Avenue, 639798, Singapore

[2] Interdisciplinary Graduate School, Nanyang Technological University, 50 Nanyang Drive, 637553, Singapore

[3] School of Mechanical and Aerospace Engineering, Nanyang Technological University, 50 Nanyang Avenue, Singapore 639798, Singapore.

[4] Singapore-HUJ Alliance for Research and Enterprise (SHARE), Campus for Research Excellence and Technological Enterprise (CREATE), 1 Create Way, 138602, Singapore

Title

Emerging Thermal-Responsive Materials and Integrated Techniques Targeting the Energy-Efficient Smart Window Application

ToC figure

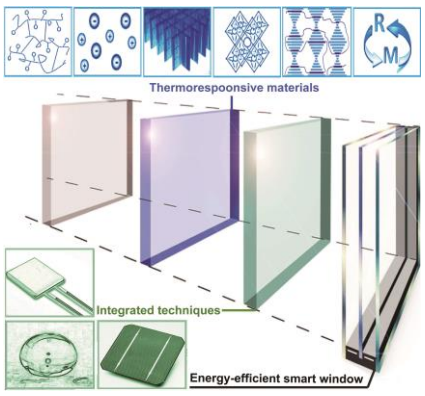

55 mm broad × 50 mm high